ELSEVIER

RESEARCH: Review

Fundamental comprehension, synthetic procedures and catalytic applications of high entropy oxide nanomaterials

Qishun Wang [a,b], Xiangwen Liu [c,*], Daping He [d,*], Dingsheng Wang [a,*]

[a] Department of Chemistry, Tsinghua University, Beijing 100084, China
[b] State Key Laboratory of Rare Earth Resource Utilization, Changchun Institute of Applied Chemistry, Chinese Academy of Sciences, Changchun 130022, China
[c] Institute of Analysis and Testing, Beijing Academy of Science and Technology (Beijing Center for Physical and Chemical Analysis), Beijing 100094, China
[d] Hubei Engineering Research Center of RF-Microwave Technology and Application, School of Science, Wuhan University of Technology, Wuhan 430070, China

Improve existing catalyst systems and create new catalytic nanomaterials *via* high entropy design strategy has been an emerging topic in field of material. High entropy oxides (HEO) possess unique properties, resulting in a complexity of the localized environments and expected wide adjustability, owing to the "cocktail" effect. However, oxides exhibit quite different behavior to their characteristics after the replacement of ≥5 elements in cation sites comparing to the condition of alloy. The practical applications of HEO nanomaterials are still lack of breakthrough in catalysis and remain largely unexplored. Limited understanding of HEOs, no matter the microscopic disordered composition or the mechanism behind, is primarily responsible for these problems. Herein, we demonstrate the fundamental comprehension of high entropy oxides from a structural perspective. Generally, synthetic procedures, catalytic applications and the complementation with single atoms of HEOs are elaborated in detail. Representative strategies to theoretically predict and screen the potential HEOs against the massive combinations of elements are discussed in this review. Furthermore, we predict short-term and long-term directions and present our perspectives with regards to design strategies and synthesis novel HEO based catalysts in the future.

Keywords: High entropy oxide (HEO); Single-atom catalysts (SAC); Heterogeneous catalysis; Lattice distortion; Non-trivial structure

Introduction

From conventional alloy to high entropy

Since the proposal of concept in 2004 [1,2], high entropy alloys (HEA) have endowed a new field of material science, owing the unique properties and innovative strategy in material design [3,4]. The definition of HEAs could be controversy but there are two commonly accepted definitions, according to several compositional requirements or meet the criterion of entropy [5]. That is single phase and equimolar, requiring at least five principle elements, or a configurational entropy (S) larger than 1.61R or 1.5R (where R is the gas constant), respectively.

As the understanding deepens in field of alloy, HEAs are also divided into two generations [6]. Its initial definition on composition was found too strict to the range of HEAs. Relaxed restrictions on HEAs compositions, non-equimolar, dual or complex phase and consist of at least four principal elements, are proposed and named as 2nd generation HEAs. Correspondingly, HEAs under the strict definitions are defined as the 1st generation. Conventional alloys possess composition points around the corners of phase diagram, while the HEAs are located at the center regions where the materials are poorly known to us [7].

* Corresponding author.
E-mail addresses: Liu, X. (liuxiangwen@bcpca.ac.cn), He, D. (hedaping@whut.edu.cn), Wang, D. (wangdingsheng@mail.tsinghua.edu.cn).

 https://doi.org/10.1016/j.mattod.2023.10.007

The concept of "high entropy" was also extended to other type of materials and nano field subsequently [8–10]. Referring to its initial definition, variety of compounds with multiple equal molar components are proposed and synthesized other than HEA, collectively referred as high entropy materials (HEM), including oxides (HEO) [11,12], carbides, nitrides, borides (the foregoing materials also referred as high entropy ceramics, HEC), hydroxides [13], selenides [14], coordination compounds [15], salts [16], etc. meanwhile, other structure, such as amorphous oxide [17], metallic glasses [18–21] and intermetallic compounds [22] are also be discovered.

Tradeoff between entropy-driven stability and ≥5 components

In contrast to the metallic bonding in alloys, HEMs are formed by various types of bonds, such as ionic, covalent, or even coordination bonds. The elemental sites in specific phase of HEA are equaled but turned to distinct and complicated in other compounds. Taking the multiary oxide as example, stoichiometric metal and oxygen atoms distribute in the lattice by a specific configuration *via* charge balance, moreover, multivalence of cations and their coordination numbers created multisites or M—O units within single phase. Furthermore, mono- or multisite could be replaced with multicomponent, respectively. Some oxides easily form defects and vacancies. In addition to configuration, disorder originated from dislocations additionally contributes in the total entropy [23]. Such situations broaden the field of compounds, however, resulting in vague definition of HEMs other than HEAs, not only to the compositional definition but also raising controversy for the calculation of configurational entropy.

Meanwhile, the entropy stabilized material is a correlative but different concept, although the use of "high entropy" materials is more common and both concepts are interchangeable in some cases [12]. The first proofed entropy stabilized oxide (ESO) was synthesized in 2015 [24]. The concept was highlighted due to the entropy-driven stability and reversible solid-state transformation. The Gibbs function of ESOs suggests that the negative ΔG is predominantly influenced by the larger configurational entropy rather than conventional enthalpy, resulting in high temperature favored stability [25]. Therefore considering the strict definition, most ESOs are thermodynamically metastable at relative low temperature (Of course, a few counterexamples are discovered) and tend to transform to multi-phase during the annealing process.

Demonstrated by the theoretical studies, the choice of five elements for defining "high entropy" is not arbitrary but rather the "sweet point" [26]. As the number of elements exceed five, the entropy raises while the enthalpy effect on ΔG is further weakened. As for oxides, the effect on configuration entropy by adding number of metal elements is weakened due to the fixed oxygen in the certain site of the oxide lattice [27]. Furthermore, entropy calculations, especially for multiary oxides, can be confusing. Take the simple binary oxide with fluorite structure and five equimolar of cations as example, the configuration entropy per formula unit (1.609R), cation (1.609R) and atom (0.536R) calculations give different results, which would be more ambiguous for ones with multisite. Attempt for inspection the range of HEOs was also made by establishing entropy metric, which considers the influence of sublattice but still weak relation with entropy-driven stability [28]. While oxides such as triple perovskites or heavily doped rare earth crystal [29] (e.g., garnets, melilites) have gathered quite a lot elements in their cation sites and obviously derive a comparable configuration entropy with aforementioned materials, but these oxides could not be considered as HEO and maintain their phase in the single crystal growth with quite small temperature gradient [30]. Is the criterion of entropy-driven stability fully included by the criterion of ≥5 components? Surprisingly, ESOs exist in nature and are also found in the slag of blast furnace steelmaking, even the limit of five components are broken with exception of some ternary spinel type oxides, as retraced in early reports [27].

Since the first reported HEA and ESO/HEO, their research fields both garner significant attention and broaden respectively [31–35]. Their characteristics and definition have deviated from each other for the emerging materials in different fields. Due to the customary, HEO becomes the most widely used concept and lots of researchers still analogize the definition of 1st generation HEA, which can be roughly expressed as the multicomponent oxides with five or more equimolar components taking the place of the initial components and forming single phase, to describe their materials. At the same time, the coexistence of multiple definitions will continue before thoroughly understanding the field of HEMs and entropy-driven stability.

Properties gained from high entropy

Four core effects: entropy effect, distortion effect, cocktail effect and sluggish diffusion effect are summarized for HEAs for their unique properties [36]. For oxides, although selected calculations present a configuration entropy just falling in the low to medium entropy range defined for alloys, they still exhibit similar changes in mechanical, physical and chemical properties, but distinguish from the range of traditional monocomponent materials [11]. These oxides also perform a reversible phase transformation during annealing process and are successfully prepared using synthesis strategies modified from those of HEAs [37]. High entropy also provides HEOs with unique properties in many aspects related to oxide characteristics.

In terms of structure, the first prepared HEO (MgCoNiCuZn)O has rock salt structure while the common phases of CuO and ZnO are not the same structure [24]. Moreover, another HEO $(GdTbDyTmYbLu)_2Si_2O_7$ with six components in specific site doesn't share its γ-$Y_2Si_2O_7$ structure with any of the $Ln_2Si_2O_7$ formed by the six individual elements [38]. As for the valency, a single perovskite HEO could gather five different valences (Ba(ZnYbTiNbW)O_3) or have no tetravalent cations (Ba(YbYGaNbW)O_3) in a tetravalent site [39]. For structures in multiary oxides, such as perovskite (ABO_3), spinel (AB_2O_4) and pyrochlore ($A_2B_2O_7$), the A-site and B-site can be simultaneously replaced with multiple elements amount to ten totally [40,41]. HEOs could also support and stabilize materials with unstable valence. Take the well-studied (MgCoNiCuZn)O as example. The Au species could dissolution in the HEO lattice despite of its intrinsic inertness [42]. The Cu selectively precipitated and formed $CeCuO_x$ with higher trivalent ratio after ball milling with CeO_2 [43]. Another inherent notion that HEMs thermodynamically favor at high temperature and are metastable therefore unstable after annealing, seems not working for some HEOs, especially rare-

earth based ones. $(GdTbDyHoEr)_2O_3$ is able to irreversibly maintain a high entropy structure in annealing, even at a quite high temperature of 1650 °C, and has phase stability contrary to the of the individual oxides of components [44]. Should be noticed that this HEO has a relatively simple structure of cubic bixbyite, with all cations randomly distributed in the only sites. The five lanthanide cations have similar ionic radii ranging from 0.89 to 0.94 Å, which probably results in a lower internal strain, in turn enhancing its stability. Single crystals of $(LuYHoNdLa)_2O_3$ and $(LuYGdNdLa)_2O_3$ with a single monoclinic B-type phase were also grown [30]. Another long-term annealing test showed that fluorite type $(HfZrCeYYb)O_{2-\delta}$ remain stable over a fairly wide temperature range, affirming adequate stability in practice [45].

Bulk materials to nanocatalysts

Oxide based materials are of great significance for heterogeneous catalysts and supports for hybrid materials, especially precious metal catalysts. The interaction between oxides and metals plays important role in the catalytic properties [46,47]. The effects of HEO bring the unprecedented wide adjustability to basic characteristics, thus HEOs have promised as candidates for addressing long-standing problems in the field of catalysis.

Apart from the particles and clusters, single-atom catalysts (SAC) have been frontiers in this field, attracting substantial attention [48–52]. One of the most fascinating aspects of HEOs is their wide adjustability as supports, which arises the advantages along with the maximized atom utilization, undercoordinated active centers and quantum size effects of SACs [53,54]. The combination of both emerging material concepts provides new approaches to low-cost, greener and more efficient catalysis.

Catalytic applications accounted for a large proportion of researches on HEMs [36]. HEOs benefit from aforementioned properties providing new material design strategy beyond traditional doped or hybrid materials with limited major component and bring the following advantages in catalysis field.

1. Complex structural changes are enabled by slight component tuning, greatly affecting the properties and extending the range.
2. Abundant of defects, vacancies, high strain of M—O bonds and lattice distortion are easily generated in the structure, resulting in similar properties to those of amorphous materials [37].
3. Localized disorder cations distribution creates multiplicative number of microenvironments inside and on the surface of the material organed from valence differences of cations and diverse sites, bringing more complex situations compared to M—M bonds in HEA [27].

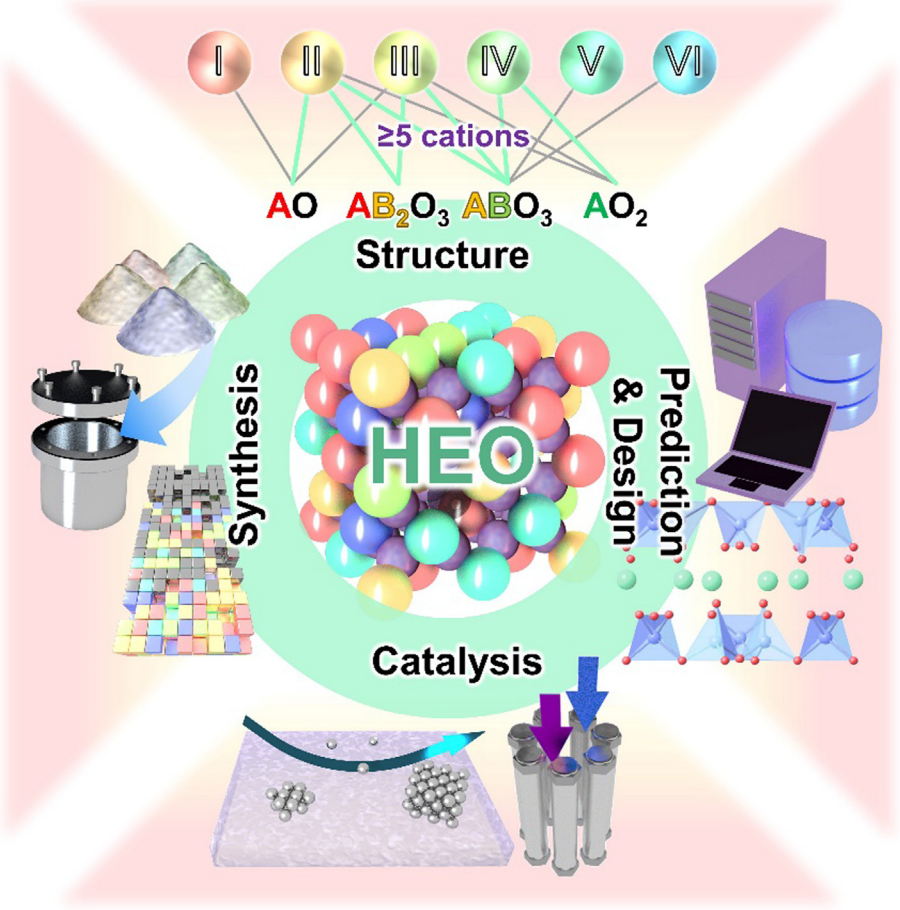

SCHEME 1

Schematic illustration of high entropy oxides in nanocatalysis.

4. Non-trivial structures for the monocomponent are allowed and provided with high localized tension. A diversity of electronegativity could coexist in specific site *via* combining non-constitutive valences.

This review will discuss nanoscale morphology, synthetic procedures, structures and catalytic properties, and look ahead the structural design, complementation with SACs and perspective for HEOs in nanocatalysis (see Scheme 1).

Synthesis

Template sintering method

Sintering is commonly used in HEO fabrication, which is still a typical and common method for nanosized HEOs. Traditional solid-state sintering usually involves the ball milling process to make the precursor oxides uniformly mixed and longtime high temperature calcination for sintering, with optional compression step before or during sintering process. The obtained materials are usually bulk or solid particles with high grain size and low specific surface area. The compression step make further efforts on reducing porosity and enhancing crystallinity, which is particularly important for the application of bulk materials [41]. Take the (MgCoNiCuZn)O as example, a minimum sintering temperature at about 900 °C is required for the phase formation from oxide precursors *via* solid-state sintering, and its single phase will be destroyed when annealed at about 700 °C.

Salts such as carbonate, nitrate, acetate and acetylacetonate, or even metal complexes, MOFs, other types of HEM (e.g. alloy [55] and hydroxide [56]) can also be used as precursors [55,57]. According to the precursors, the synthesizing temperature of HEO could be as low as 500 °C. Xing and coauthors fabricated metal-PVP precursor by electrospinning and subsequent calcination, obtaining all rare earth HEO $(YYbSmEuEr)_2O_3$ with bixbyite (*Ia-3*) structure [58]. Synthesis methods bring considerable performance differences. However, the products *via* solid-state sintering are always not suitable for the field of catalysis where structured nanoparticles and narrow distribution are desired [59]. The specific surface area decreases (Fig. 1a) and active sites aggregate after longtime sintering, even with nanosized precursors. So modifying the synthetic procedure by adding removable templates to separate the particles is a feasible way.

Dai's team chose the SiO_2 as removable hard-template, which could be etched by NaOH aqueous solution (Fig. 1b). Fumed silica was ball-milled with metal salts and together pyrolyzed at 900 °C. After etching process, rich porosity and atomically dispersed Pd are formed and the obtained fluorite type Pd_1(CeZrHfTiLa)O_x HEO reached a pretty high specific surface area of 162.1 m^2g^{-1} [60]. They also use soluble NaCl as hard-template in synthesis of perovskite type $Zr_{0.5}(NiFeCuMnCo)_{0.5}O_x$. NaOH and NaCl were added to chloride salts and the anions exchanged during balling and subsequent calcination at 500 °C. Finally, the sodium salt could be removed by washing, remaining pores with specific surface area up to 84 m^2g^{-1} [61]. Post-process of template removal adds the complexity of the porous HEO synthesis. Also the template materials need to maintain stable during calcination (for instance, SiO_2 reacts with many transition metal oxides at high temperatures) but easily etched or washed, so the choice of etchant and template is limited.

To let the precursors forming self-template maintains the simplicity of the solid-state synthesis and enables the fabrication of nano-structure. Zhou and Huang's team chose molten glucose as the self-template and inspired by "black powder", additional ammonium nitrate was added along with metal nitrates which generated large amount of gas by heating, blowing molten glucose to form a foam structure. By further carbonization and calcination, the carbon was fully oxidized and removed, thus ultrathin porous oxide sheets were obtained (Fig. 1c) [62]. The strategy could synthesize a wide range of monocomponent oxides and was also extended to two kind of HEOs, including cubic bixbyite type $(ErGdYbSm_{1.2}Y_{0.8})_2O_3$ and spinel type $(CoMnNiCrFe)_3O_4$, remaining their single phase. Similar strategy was developed by Dong's team, they adopted the deep eutectic solvent which is consist of glucose and urea. Owing to the low melting point, the liquid can directly dissolve metal salts at operable temperature. In addition to the carbonization of glucose, the urea component also acts as a foaming agent similar to ammonium nitrate. The precursors were carbonized to black foam by directly microwaving and calcined to obtain HEOs (Fig. 1d) [63]. Solvents helps to mix the metals more uniformly than ball milling. Furthermore, by varying the metal concentration, different morphologies of nanowires and nanosheets can be tuned. This method is applicable to a variety of HEOs, including rock-salt type (5M)O, spinel type $(5M)_3O_4$ and perovskite type La$(5M)O_3$.

Soluble salt precursors could also be encapsuled in porous templates *via* simple solution process. Qiao's team used oxidized graphene sheets as cation adsorber for synthesizing porous lamellar structured rock-salt type (5M)O [64]. A relative high specific surface area of 42 m^2g^{-1} was achieved. There are also HEOs deriving from MOFs [65] and electrospinning [66] by calcination. These methods basically maintain the original structure to avoid sintering, thus creating more interface and abundant surface defects, which are beneficial to catalysis.

Combustion method is a variant of thermosynthesis. Organic molecules such as citric acid, glycine, are used as incendiary agent, which have high fuel to oxidizer ratio and good coordination property. By forming gel with metal salt precursors, the molecules help to distribute the ions evenly despite of valence difference and form the template. The auto combustion assisted by low temperature heating completes the reaction violently. With the aid of glycine, Gautam and Ahmad presented the synthesis of rock-salt type (5M)O at a low trigger temperature of 185 °C without demand of post-annealing [67]. Nevertheless, combustion reaches a high temperature but only for a short period, so annealing may still be required to ensure high crystallinity.

Rapid heating and cooling method

Regular laboratory furnaces are enough for meeting the requirement for thermal synthesis of HEOs in most time, to achieve a high temperature gradient is still highly desired. The relatively low temperature gradient and long heating time are always unfavorable for nano size of materials. A quick quenching step in HEO synthesis not only quenches the metastable phase, but also

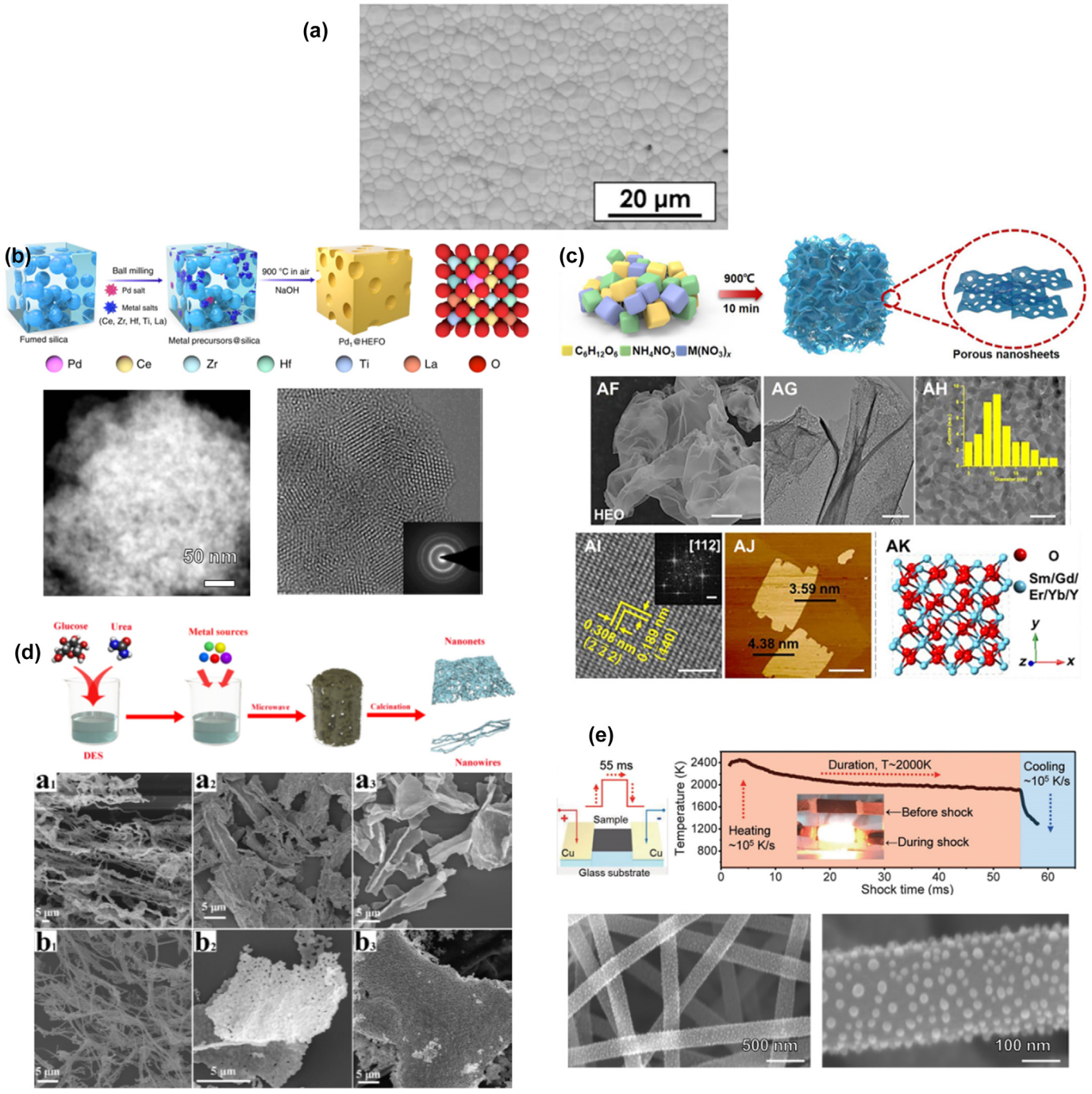

FIG. 1

Schematic illustration of temperature driven synthesis and morphology of corresponding HEOs. a) A typical surface morphology of HEO bulk from solid-state sintering. Reproduced with permission [68]. Copyright 2021, Elsevier. b) Porous SAC/HEO synthesized via hard-template. Reproduced under the terms of the Creative Commons CC BY license [60]. Copyright 2020, Springer Nature. c) HEO sheets synthesized via self-template. Reproduced under the terms of the Creative Commons CC BY license [62]. Copyright 2022, AAAS d) Sheet and wire shaped HEO synthesized using deep eutectic solvent. Reproduced with permission [63]. Copyright 2021, Springer Nature. e) HEO particles supported on CNTs synthesized via Joule heat [69]. The schematic illustration of Joule heat is adapted from Ref. [70] and shows the situation of HEA synthesis. Reproduced with permission. Copyright 2021, Springer Nature. Copyright 2018, AAAS.

helps to obtain defects, reduce the phase separation and grain size, especially for nanomaterials. But operation like removing the as-heated crucible from working furnace and cooling in air are not follow the rules with quite risk. For safely and effectively forming high heating and cooling gradients in sintering, various methods including laser irradiation [71,72], spark plasma sintering (SPS) [73], and heating by arc, current [74], microwave [75] or oxygen plasma are practicable for HEM synthesis and made available for HEO, but not all of these suitable for nanocatalysts.

To accurate a similar reaction pathway as solid-state sintering, localized heating methods with high power density acting upon small amount of samples are proposed. Wang's team adopt

microwave synthesis for HEO by grinding CNTs and metal acetylacetonates. (RuNiMoCrFe)O_x particles in ~6 nm size were uniformly supported on CNT supports, which also acted as microwave absorber [75]. Current heating method, named with Joule heat invented by Hu's team provides ultrahigh temperature gradient of heat/cooling (magnitude of 10^5 K/s) and ultrahigh pyrolysis temperature (up to about 2000 K), allowing the material to be synthesized in less one second (Fig. 1e) [69,70]. More ideally, this method is suitable for a wide range of HEMs by varying the precursors and the atmosphere with uniform size distribution. The heating time could be precisely controlled using a programmable DC power supply. However, conductive supports are essential in this method, such as carbon fiber or high melting point metal foils [76]. And temperature changes cause sharp changes in resistance, making it impossible to precisely maintain the heating power. Another challenge is the poor uniformity for temperature due to the uncontrollable current distribution, despite the temperature which this method could reach is high enough to ensure the transformation of HEO phase. The HEO products are also inconveniently separated from the support, Coincidentally, for applications such as electrocatalysis, these conductive supports alone with the HEO could be directly used as self-stand electrode.

If we keep the basic structure of laboratory furnaces, but allowing the sample to quickly pass through the heating zone, it is also possible to accurate heating and cooling gradient.

The spray pyrolysis method provides such resolution. Small isolated droplets of the precursor solution could be generated by collision nebulizer and move through a high temperature zone. The droplets evaporate and shrink by constraint of surface tension, finally remain uniform spherical solids, avoiding size growth of the products during the traditional pyrosis process. By addition of ammonium nitrate or urea, porous [77] and hollow [78] morphologies are obtained. This method could achieve continuously synthesis with size control ability by tuning the concentration or droplet generation.

Tube furnaces widely used in spraying synthesis have many disadvantages. Gases are not good conductors of heat, so uneven heat transfer in the heating chamber become a very serious problem. Hu's team adopted the micro channel from carbonized wood heated by Joule heat to achieve a uniform temperature distribution in addition to an ultrahigh temperature of 2000 K. Both HEA and HEO could be synthesized by this method [78]. Another problem is the diffusion of the spray difficult to control and the material tending to adhere to the tube walls, leading to low yield and difficulty in collecting, which could also combine with electrostatic spray to control droplet size and limit its motion. Endogenous heating could simultaneously prevent the thermal conduction and tube wall problem. By ejecting and reacting the precursors in the petroleum gas flame heat source of more the 2000 °C, flame spray pyrolysis produced about 10 nm size fine powder [79]. The plasma heating [80] could reach even higher temperature and promotes HEO synthesis.

Non-temperature-driven synthesis

Synthesis strategies of HEO under mild conditions are highly desired. The synthetic temperature of hydrothermal method can be significantly lower than the solid-phase synthesis temperature, but it deviates from the thermodynamic formation temperature of HEO and may causes poor crystallinity or amorphous produtcts [81] unless mediating by strong agent (such as high concentration alkali, oxidant) or post-sintering process. A spinel type HEO with hollow sea urchin morphology were synthesis by hydrothermal method at 120 °C for 12 h *via* ostwald ripening (Fig. 2a), achieving a very high specific surface area of 199.93 m^2g^{-1} poor crystallinity [82]. The poor crystallinity could be solved by post annealing, which effectively reduces the calcination temperature [83,84] and retains the controllable morphology formed by hydrothermal synthesis [13]. Wei's team used a ligand-assisted hydrothermal method to fabricated polymer spheres, solid and hollow mesoporous HEO were then obtained by relative low temperature calcination at 400 °C or 600 °C [83]. Li's team adopted a viscosity mediated micelle assembly strategy and fabricated dendritic mesoporous HEO by two-step hydrothermal and calcination (Fig. 2b). Up to denary of rare earth element were formed with uniform dendritic structure [85].

Apart from the traditional hydrothermal or solvothermal reactions, more reaction media are adopted. Zheng's team choose ionic liquids as solvent and HEO were one-step synthesized with the aid of NaOH, the ionic liquids significantly reduced the particle size due to the improved Ostwald ripening [86]. Iwase and Honma also invested a one-step hydrothermal synthesis for spinel type HEO fabrication using supercritical water at 400 °C for 15 min as the solvent, obtaining small particles around 20 nm with high crystallinity (Fig. 2c) [87].

Mechanochemical and sonochemical process are also adopted in HEO synthesis. As mentioned in solid-state sintering procedure, ball milling is commonly used for mixing the precursors. The high-energy ball milling technique can achieve localized high temperature and pressure for atomic-level mixing, which is also adopted in largescale synthesis of SACs [88]. This method also emerges as fast and solvent-free synthesis, achieving direct chemical transformations without further processing through high energy of mechanical collision. Dai's team endowed rapid synthesis of HEO in 2 h operated at room temperature, and ball-milling accelerates the diffusion of M—O bonds from oxide precursors. As high as 5 wt% Pt or Ru were loaded on (NiMgCuZnCo)O, coexisting of single-atoms (SAC) and clusters [89]. Zhang's team modified the mechanochemical synthesis with double replacement and self-redox of the precursors [90]. The chloride salts (except Mn) exchanged with NaOH and partial Co oxidized by $KMnO_4$ after ball milling, forming amorphous hydroxide and NaCl. Porous (Co_3MnNiCuZn)O_x HEO with spinel structure are obtained after washing NaCl and calcination at 600 °C. Dai's team also developed ultrasonication-assisted synthesis, further shorten the time to 10 min. By sonicating the precursors in high concentrated NaOH, porous perovskite type HEOs are obtained with specific surface area up to 85.5 m^2g^{-1} (Fig. 2d) [91].

Oxidative etching method transforms the substrates into HEOs. Qiu's team used a dealloying process of etching Al-rich HEA by NaOH. The obtained HEO had spinel lattice according to TEM and up to octonary cations, but with weak peak in XRD analysis duo to the poor crystallinity and small grain size [92]. By adopting precious metal in the Al-riched HEA systems,

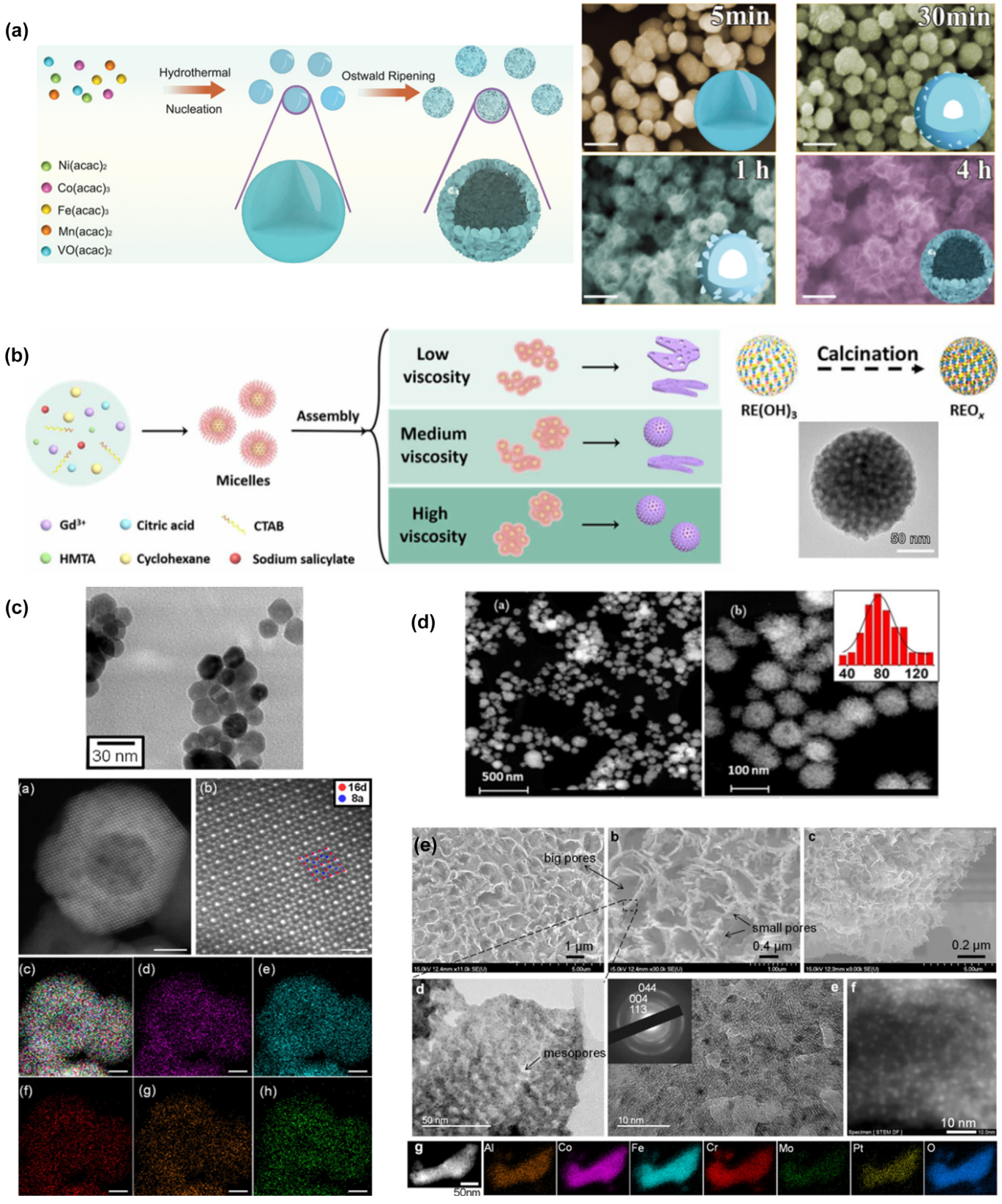

FIG. 2

Schematic illustration of non-sintering synthesis and morphology of corresponding HEOs. a) Hollow HEO spheres synthesized via ostwald ripening. Reproduced with permission. Reproduced with permission [82]. Copyright 2020, Wiley-VCH. b) Dendritic mesoporous HEOs synthesized via micelle assembly strategy. Reproduced under the terms of the Creative Commons CC BY license [62,85]. Copyright 2022, AAAS. c) High crystallinity HEO synthesized via supercritical hydrothermal method. Reproduced with permission. Reproduced with permission [87]. Copyright 2022, ACS. d) Porous HEO synthesized via ultrasonication. Reproduced with permission [91]. Copyright 2020, Wiley-VCH. e) Mesoporous Pt/HEO synthesized via dealloying of HEA. Reproduced with permission [94]. Copyright 2021, ACS.

Ag, Pt or even the precious metal based HEA of PdPtCuAgAu retained as nanoparticles and uniformly dispersed on the HEOs, which could be nanowire, nanorod, or rugged morphology with rich porosity depending on the shape of the intermetallic phase (Fig. 2e) [93,94]. Huang and coauthors developed an two step electrochemical oxidation method to synthesize (CoCeNiFeZnCu)O_x from CuS [95]. The other cations firstly exchange with Cu ions, and then converted by electrochemical oxidation, forming the CuO structure and remaining the nanoplate morphology of initial CuS.

Characterization

The multicomponent nature brings new difficulties in investigating the structure of HEOs, especially for nanocatalysts. A crucial point is to detect the element of individual atoms and M—O—M bond relations. Unfortunately, most characterizations give the average data within certain area, ranging from nanoscale to bulk. Even some techniques could reach sub-ångström resolution at the atomic scale, there are still problems that no enough information to detect elements, for example, contrast in aberration-corrected scanning transmission electron microscope (AC-TEM) is related to atomic number of elements but inadequate to distinguish them. Nevertheless, owing to improvement of frame rate in the sampling and computational photography, tomography is promised to reconstruct the 3D structure. Or quite thick samples are required to ensure the signal–noise ratio, such as X-ray absorption spectroscopy (XAS) [96], which gives average data from macroscopic samples, X-ray energy-dispersive spectroscopy (EDS) and electron energy-loss spectroscopy (EELS), which both require high crystalline to reach their resolution limit and prefer position with ∼nm sample to collect data point and output 2D patterns. Scanning probe microscopy (SPM) has enough mechanical resolution in atomic scale, but quite a lot of modes require the conductive samples. The atomic force (AFM) mode doesn't fit the mechanism research, which acquires no information related to element distribution or electronic structure.

So far, only atom probe tomography (APT) is adapted to determine the exact 3D atomic compositional mapping in 3D spatial of HEOs (Fig. 3a) [97]. APT uses time-of-flight mass spectrometry (ToF-MS) to collect a huge data set from atom evaporation in a destructive process towards sample induced by a pulsed laser and reconstructs nanoscale cloud mapping of individual atoms [98]. APT provides information including chemical segregation, dislocations in defects, grain boundaries and agglomeration of elements, which are hardly obtained in common characterization. Combining APT with microscopies and spectroscopies could comprehensively reveal the structure of HEO, which will provide new insights into the structure of HEOs and inspire future research in the field of catalysis.

Powder X-ray diffraction (XRD) also plays important role in characterizing HEOs. Its patterns present strong evidences regarding to the phases and structures. Should be noticed that identifying pure phase materials from HEO candidates *via* XRD could be challenging, as multiphase materials may diffract indistinguishable peaks due to same structure and slightly change in lattice, which demands further refinement for accurate identification. To achieve high signal–noise ratio in HEO characterization, synchrotron X-ray methods [99] and neutron diffraction [100] take effect and could detect extra short- and long-range order information for delving deeper into the structural mechanism.

Due to the complexity of simulation and the difficulty for accurate characterization of active sites, Lack of mechanism researches limited our understanding in catalytic applications of HEOs. Based on current techniques, researchers still revealed some differences compared to traditional oxides. Pan's team combined the data from AC-TEM (Fig. 3b) to estimate elemental fluctuation and charge distribution at atomic scale of perovskite type HEOs [101]. Gao's team visualized the fluorite type HEO formation *via* in situ TEM, showing the surface evolution and localized clustering with nonuniform elements concentration in 10 nm scale region [102]. Ultrahigh density of dislocations ($\sim 10^9$ mm^{-2}) in variety types of HEOs were observed by Wan's team using geometric phase analysis, which had high correlation with the configuration entropy (Fig. 3c) [23].

Structure

The rock salt structure (cubic, *Fm-3m*) HEOs possess chemical composition of AO (the A and B present different cation sites, similarly hereinafter), principally transition metal elements [24]. The experiment number of this compound (MgCoNiCuZn)O is J14 by the first discoverer Rost. He and coauthors also synthesized and tested the 4-component medium entropy materials by removing every component and concluded that Cu plays important role in stabilizing the structure. The specificity of Cu was also illustrated by Anand's research [103]. GULP simulations focusing the J14 system showed the enthalpy loss is quite low for the increasing numbers of elements in the oxide system. The M—M bond lengths and M—O bond lengths tend to be average, thus generating a large stress for Cu and Zn elements comparing with their monocomponent oxides. However, it is interesting to note that the common phase of oxide for these two elements are exactly not rock salt structures in opposite with other 3 elements. Probably due to the relative high difference of transition metal ion radius, only a few divalent ions, such as Fe and Mn, could enter the lattice of rock salt structured HEO [76]. There are also HEOs which share components close to the rock salt type J14 but have different structure. Huang and coauthors developed a series materials, one of which only replaces Mg element by Fe (divalent oxide FeO is still a rock salt structure), but has a single phase CuO structure (monoclinic, *C2/c*) [95].

In addition, LiF and NaCl could also dope in rock salt structured HEO and maintain its single phase, which inspires applications in ion conduction and ion batteries. Lun et al. searched and synthesized possible HEOs with rock-salt structure by density functional theory (DFT) [104]. Due to the cationic disordered structure, these Li contained HEOs have very high capacity as cathodes. Besides these, the synergy of monovalent element (Li, Na) and trivalent element (Mn, Sc, Ge, etc.) maintains the charge balance and single phase but extend the range of feasible ions in rock salt structure HEO. Monovalent and trivalent ions (allowing a small amount of other valence ions) can also form layered $NaFeO_2$ structure HEO (hexagonal, *R-3m*) with potential energy storage applications [105].

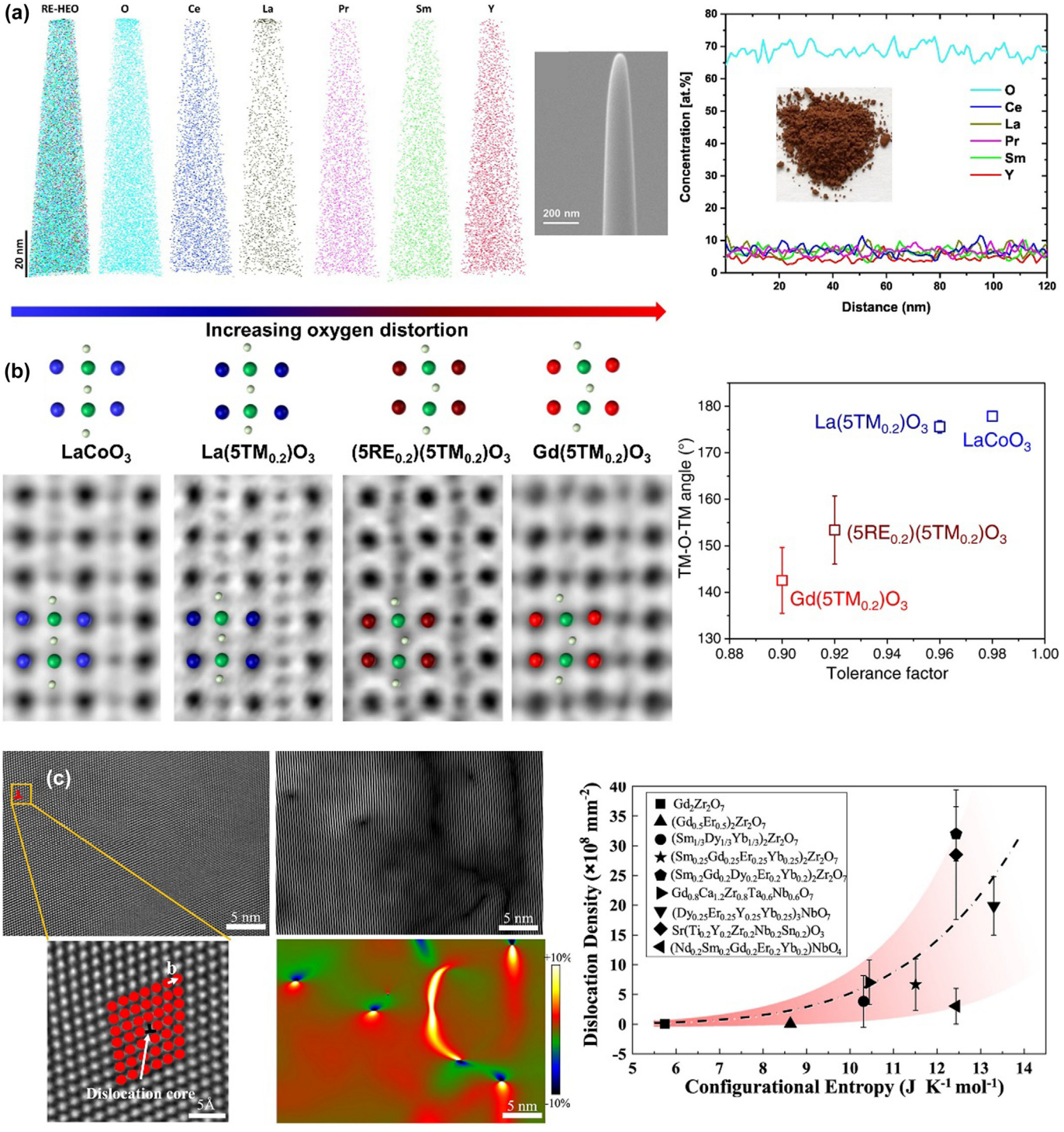

FIG. 3

Techniques for investigating HEOs at the atomic scale. a) Atom probe tomography and illustration of the test sample. Reproduced with permission [97]. Copyright 2019, Elsevier. b) AC-TEM based measurement. Reproduced under the terms of the Creative Commons CC BY license. [101] Copyright 2022, Springer Nature. c) Geometric phase analysis of $(SmGdDyErYb)_2Zr_2O_7$ and relation of dislocation density and configurational entropy. Reproduced under the terms of the Creative Commons CC BY license [23]. Copyright 2022, Springer Nature.

For cations with various valence, a more complex behavior is observed when they forming HEOs. The spinel structure (cubic, *Fd-3m*) HEOs have both divalent and trivalent sites in the lattice, possessing chemical composition of AB_2O_4, where of the cations filled in but their distribution is not fully disordered owing the valency. The first spinel structure HEO of $(NiCoCrFeMn)_3O_4$ reported by Dabrowa and coauther [106] was then investigated by Sarkar and coauthors and determined to be $[Co_{0.6}Fe_{0.4}][Cr_{0.3}Fe_{0.1}Mn_{0.3}Ni_{0.3}]_2O_4$ for their chemical composition, where the Fe dispersed in both two sites [107]. This spinel HEO is magnetic

and can be used for dye degradation and detection [83]. The structure of $(Fe_xCoNiCrMn)_3O_4$ could be transformed from spinel type ($x < 3$) to α-Fe_2O_3 type ($x > 5$) with increasing the Fe content [108]. A variety of di- and trivalent transition metal ions can enter the spinel structure, including Al, Mg, Zn, Ti, etc. Some spinel type HEOs also have slightly componental different with J14, such as replacement of Zn by Fe [77] or replacement of Mg by Mn [90].

A perovskite structure (cubic, *Pm-3m*) oxide may have divalent and tetravalent cations or both trivalent cations in its cation sites. The chemical composition of perovskite structure HEOs could be diverse, which means not only transition metals, alkaline or rare earth metal elemnts could also enter its sites with formula of ABO_3.

Due to the lanthanide contraction, the rare earth oxides are easily doped with each other with common formula $(RE)O_{2-\delta}$. These rare earth oxides formed cubic structure with various space groups. The rare earth elements all exhibit the trivalence and the corresponding oxide belongs to sesquioxide, which has bixbyite structure (*Ia-3*). Specific rare earth elements such as Ce and Pr also possess tetravalence. The ceria has the fluorite structure with general *Fm-3m* space group. Tetravalent ions of non-rare earth elements such as Zr, Hf, Ti, and Sn, are able to enter the fluorite structure, where the rare earth content can be as low as 1/5 [109]. Some non-rare earth HEOs with a high average valence were discovered, such as rutile type (tetragonal, *P42/mnm*) [75].

Pianassola and coauthors investigated rare earth based HEOs and determined the role of Ce and Pr for their structure [110]. Besides the entropy effect, the redox atmosphere can also affect the structure. Ce and Pr contribute to the formation of a cubic phase in oxidizing environments. All samples without either Ce or Pr developed a single monoclinic structure. Spiridigliozzi and coauthors reported a simple model applicable to the phase prediction and found that the deviation of the elemental ion radii is crucial for the formation of a single crystalline phase, using standard deviation to measure the cation radii dispersion [111]. Systems with standard deviation $s > 0.095$ for the distribution of cation radii result in the formation of a fluorite structure. For $s < 0.095$, first a biphasic system is formed, and then a single-phase bixbyite structure is formed. Besides these, rare earth based HEO can also be transformed into pyrochlore phase (cubic, *Fd-3 m*) [112].

Catalysis

Thermocatalysts for oxidation

Some oxides inherently possess catalytic activities, so it is not surprising that HEOs perform well for these reactions. Chou's team reported fluoride type HEO $(CeLaPrSmY)O_{2-\delta}$ in absent of precious metals with better CO oxidation properties than pure CeO_2 [113]. CO oxidation is the common probe reaction adapted in the research. Its mechanism over J14 nanocatalyst was detected different from the component oxide alone. Fracchia and coauthors invested CO oxidation behavior of pure (MgCoNiCuZn)O by *operando* XAS and a reversable Cu(I)/Cu(II) redox cycle was observed, indicating a difference in electronic structure. The HEO was highly active at high temperatures in different atmospheres, and also exhibited vapor resistance [114]. The spinel type $(CuNiFeCoMg)O_x$-Al_2O_3 catalyst also showed good sulfur tolerance in CO oxidation [77]. Dai's team doped 25% of cation in CeO_2 with transition metals using colloidal synthesis [115]. The HEO dopants induced oxygen vacancies and activated lattice oxygen, which is proofed by ^{18}O isotope exchange, promoting good CO oxidation property and resistance to poisoning and vapor.

SACs occur good poisoning resistance, unlike the clusters. Adopting the HEOs as substrate further enhances the ability. Zhao and coauthors prepared a Pt SAC-HEO/Al_2O_3 hybrid catalyst for CO oxidation. The spinel type HEO $(CoNiFeZnCu)O_x$ assisted for the vapor resistance and Pt stabilization, the Pt transformed to oxidic-metallic phase but maintained the activity compare to non-HEO samples [116]. Dai's team also prepared HEO/Pt SAC with good CO oxidation property and thermostability at a relatively low loading of 0.3 wt%, which remained highly dispersed after high temperature reduction [117]. Another porous HEO $(CeZrHfTiLa)O_x$ could stabilize Pd SAC, which enters the fluorite lattice, but the process is forbid with CeO_2 alone [60]. The change from monocomponent to multicomponent caused shift of diffraction peaks in XRD. According to XPS, Pd is tetravalent, but XAS results indicated that Pd is between zero and bivalent. The phenomenon could be the result of abundant surface oxygen vacancies, which are able to stabilize the Pd SAC and consistent with the conclution of other studies [118,119]. CO oxidation was tested and the HEO/Pd SAC exhibited low activation energy and high hydrothermal stability.

As for the HEO-based precious metal nanocatalysts, Hu's team reported a $(ZrCe)_{0.6}(MgLaYHfTiCrMn)_{0.3}Pd_{0.1}O_{2-x}$ catalyst designed according to material library from their high throughput synthesis. The precious metal contained HEO exhibited good methane combustion properties and long-term stability no matter the presence of water [69]. Dai's team discover the high lattice compression in the porous perovskite type HEO $Ru/[Ba_{0.3}Sr_{0.3}Bi_{0.4}][Zr_{0.2}Hf_{0.2}Ti_{0.2}Fe_{0.27}]O_3$. Even only a loading of precious metal as low as 0.2 wt% performed better then $BaRuO_3$ material in CO oxidation [91]. A self-regenerative catalyst concept based on HEO/Au materials was also exhibited [42]. Trivalent Au was stabilized only when existence of rock salt high entropy phase in treatment at 900 °C. The phenomenon was not appeared in non-HEO samples. Annealing at 700 °C resulted in phase separation along with Au cations diffusing out of the HEO lattice, indicating that entropy is an important factor in stabilizing Au species (Fig. 4a). Au agglomeration leaded to higher CO oxidation activity and the surface condition could be restored by sintering and annealing cycles.

Other than CO oxidation, HEO nanocatalysts are also discovered application of organics oxidation in mild condition. Shu and coauthors reported a highly defective fluorite structure $Ce_{0.5}(ZnCoMgNiCu)_{0.5}O_x$ with half of the cations all bivalent, while 50% atomic ratio doped CeO_2 with CuO is biphasic [120]. The material showed good VOC combustion properties due to the oxygen vacancies [121] and also high hydrothermal stability (Fig. 4b). The porous lamellar structured (MgCoNiCuZn)O synthesized by Qiao's team promoted good benzyl alcohol oxidation activity. They found the porous structure accompanied with multicomponent increased the density of oxygen vacancies (Fig. 4c). Removing any of the five elements

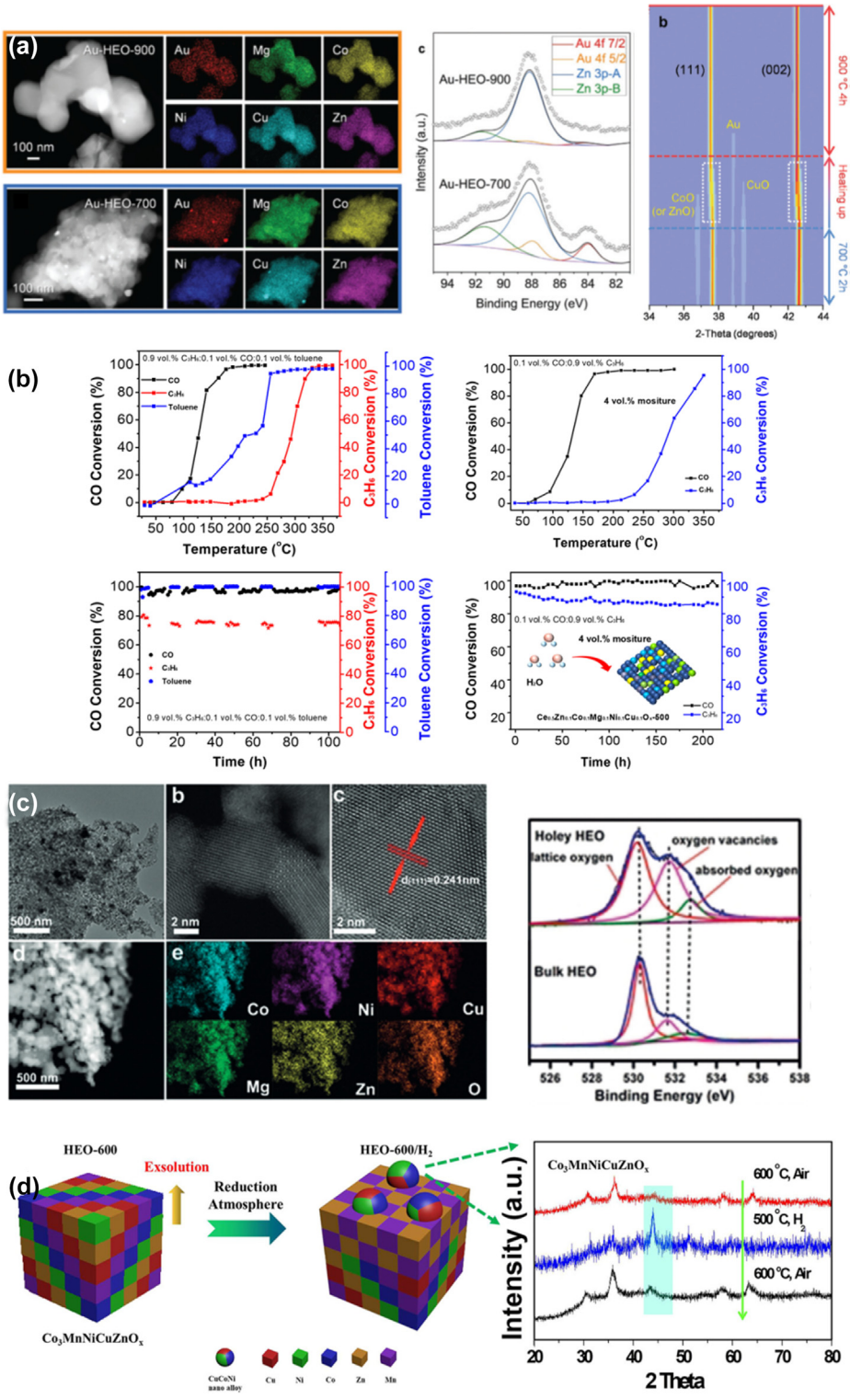

FIG. 4

a) The dispersion and valency of Au under 900 °C and 700 °C, the XRD patterns showing the structure transformation. Reproduced with permission [42]. Copyright 2020, RSC. b) VOC combustion properties and stability test of $Ce_{0.5}(ZnCoMgNiCu)_{0.5}O_x$. Reproduced with permission [120]. Copyright 2021, Wiley-VCH. c) Comparison of oxygen XPS spectra of the holey HEO with reducing components and bulk HEO. Reproduced with permission [64]. Copyright 2020, Wiley-VCH. d) Schematic illustration of self-regenerative properties by exsolution and reoxidation in $(Co_3MnNiCuZn)O_x$. Reproduced with permission [90]. Copyright 2021, ACS.

leaded to a decrease in activity, which confirmed the entropy effect affects the activity [64].

Thermocatalysts for C_1 transformations

Precious metal loaded (MgCoNiCuZn)O materials were investigated for CO_2 hydrogenation. Using mechanochemical synthesis, HEO supported highly dispersed Pt or Ru were fabricated by one-step method, promoting high loading up to 5 wt% [89]. The catalysts were used for rWGS and exhibited good sintering resistance. Under the condition of 500 °C, the precious metal maintained as SAC and cluster, and therefore exhibited high CO selectivity, usually originated from the highly dispersed sites [122]. Meanwhile, similar single-phase materials loaded with precious metal prepared by incipient wetness impregnation were unable to resist sintering and therefore prefer CH_4 production.

The spinel type porous $(Co_3MnNiCuZn)O_x$ was test in rWGS reaction and the Cu, Co and Ni elements were partially reduced, the derived catalysts exhibited good stability and self-regenerative properties (Fig. 4d) [90]. Zhang's team also reported HEO nanocatalyst $Zr_{0.5}(NiFeCuMnCo)_{0.5}O_x$ with self-regenerative alloy exsolution in reducing atmosphere and tested the rWGS reactions, achieving good sintering resistance properties for a period of 500 h [61]. Wang and coauthors reported a spinel HEO $(CoCrFeNiAl)_3O_4$ in ethanol steam reforming, reaching 81% of the hydrogen yield [123].

Electrocatalysts for water splitting

HEOs are also used in several electrocatalytic reactions, among these, the oxygen evolution reaction (OER) is one of the two half-reactions of water decomposition, which could produce green hydrogen and replace the non-renewable fossil fuel [124–126]. Liu and coauthor tested the OER activity of nanosized J14 HEO derived from electrospinning metal-PAN polymer precursors. Enhanced Co/Ni-O covalency was confirmed by compressed Co—O and Ni—O bonds (Fig. 5a) and improved four-electron OER performance with the aid of abundant lattice oxygen and oxygen vacancies [66]. Wu and coauthors used Ni foil as the conductive supports of Joule heat for (MgFeCoNiZn)O synthesis, where a little compositional difference from J14 is that Fe element replaces Cu. Atomic strain distribution pattern clearly showed uneven strain caused by Fe replacement (Fig. 5b). The continuous electronic structure of HEO could tune the d-band center to increase the OER property [76]. The same compression of the M—O bonds in HEO structure occurs with increasing components. The adsorption of OH* is crucial step in OER reaction. The volcano plot on adsorption energy showed a six component $(CoCeNiFeZnCu)O_x$ material closer to the peak (Fig. 5c) than other HEOs or monocomponent oxide which also exhibited highest OER activity and demonstrated by simulated binding energies of oxygenated intermediates. Besides rock salt structure, Wang's team tested the spinel HEO hybrid with carbon nanotubes and significantly improved the OER properties compared with pure HEO [84]. The HEO fabricated by supercritical hydrothermal synthesis had the site occupancy determined as $[Fe_{0.35}Co_{0.33}Zn_{0.32}][Mn_{0.71}Fe_{0.90}Co_{0.03}Ni_{0.36}]O_4$ by XAS analysis, which showed low Tafel slope in alkaline OER [87].

Rare-earth-containing perovskite nanomaterials have been used in OER reaction [127]. Ting's team examined the OER activities of $La(CrMnFeCoNi)O_3$ system where six samples including the multicomponent in equimolar and double dosage of each metal were synthesized and tested [128]. All samples outperformed better than any monocomponent and the non-equimolar HEO with high Co content had the highest performance (Fig. 5d), proofed by free energy of the rate-determining step and Co(III)/Co(II) ratio from DFT. The composition prediction and optimization was further invested by Okazaki and coauthors based on Bayesian optimization [129]. They gave the same conclusion that non-equimolar HEOs with high ratio of active elements performed better in OER. These compositions were all rhombohedral with *R-3c* space group and the configuration entropy calculated by formula unit belonged to the medium entropy, due to the and inactive elements (see Fig. 7c) . Besides oxides, cation sites of halide perovskites could also be replaced by five or more elements. Dai and yang's team reported a perovskite type HEMs $K(MgMnFeCoNi)F_3$, which could form oxide-fluoride solid solution with $La(CrMnFeCoNi)O_3$ and further improved the configuration entropy (Fig. 5e), endowing a new strategy for improving the activity in OER [130]. Sun's team observed the abundant surface oxygen vacancies and fast oxygen ion diffusion rate in HEO nanocatalyst $[La_{0.6}Sr_{0.4}][Co_{0.8}Fe_{0.1}Mn_{0.1}]O_{3-\delta}$, promoting OER kinetics [131]. Promoted OER by oxygen vacancies of HEO was again proofed by their subsequent research. The disordered cations in HEO nanocatalyst $[La_{0.6}Sr_{0.4}][Co_{0.2}Fe_{0.2}Mn_{0.2}Ni_{0.2}Mg_{0.2}]O_3$ reconstructed the surface, thus kinetically favoring oxygen formation *via* lattice oxygen-participated pathway [132].

Wang's team reported a rutile type HEO composite $(RuNiMoCrFe)O_x$/CNT catalyst and showed better acidic OER activities than RuO_2 [75]. Svane predicted the OER properties on (1 1 0) surface of another theoretical rutile type HEOs $(RuTiIrOsRh)O_2$ and gave the model describing the reaction pathways [133].

Electrocatalysts for other reactions

Although most known HEO-based electrocatalytic nanomaterials are used for OER reations, the researchers still found some that applied to other reactions. Liu's team reported $(CoCuNiFeMn)_3O_4$ for oxidation of ammonia with 85%+ Faradic efficiency [134]. Chen's team predicted potential HEO catalysts from DFT and synthesized the sea urchin shaped $(Ni_{0.20}Co_{0.16}Fe_{0.24}Mn_{0.18}V_{0.22})_3O_4$ comprised of ultrathin sheets. The structured interfaces and unique electronic structures promoted remarkable bifunctional N_2 reduction reaction (NRR) and OER properties (Fig. 6a) [82].

Tian's team synthesis a perovskite type HEO system in which $La_{0.7}Bi_{0.3}Mn_{0.4}Fe_{0.3}Cu_{0.3}O_3$ had the largest lattice compression, exhibiting high ORR properties and other electrochemical applications. The electron–electron couplings between the donor and acceptor cations were enhanced by cocktail effect [135]. Qiu's team reported a bifunctional electrocatalyst of spinel type Ag/$(AlNiCoFeCr)_3O_4$. The existence of Ag provided good ORR properties and also promoted the OER reaction comparing with pure HEO. Although Ag is not suitable in OER but it still significantly decreased the Tafel slopes and overpotentials [93]. A kilogram synthesis of $Pb(NiWMnNbZrTi)O_3$ was achieved by Kang's team by solid sintering. The HEO exhibited 91% selectivity in alkaline electrosynthesis of H_2O_2 over a wide potential while the low-

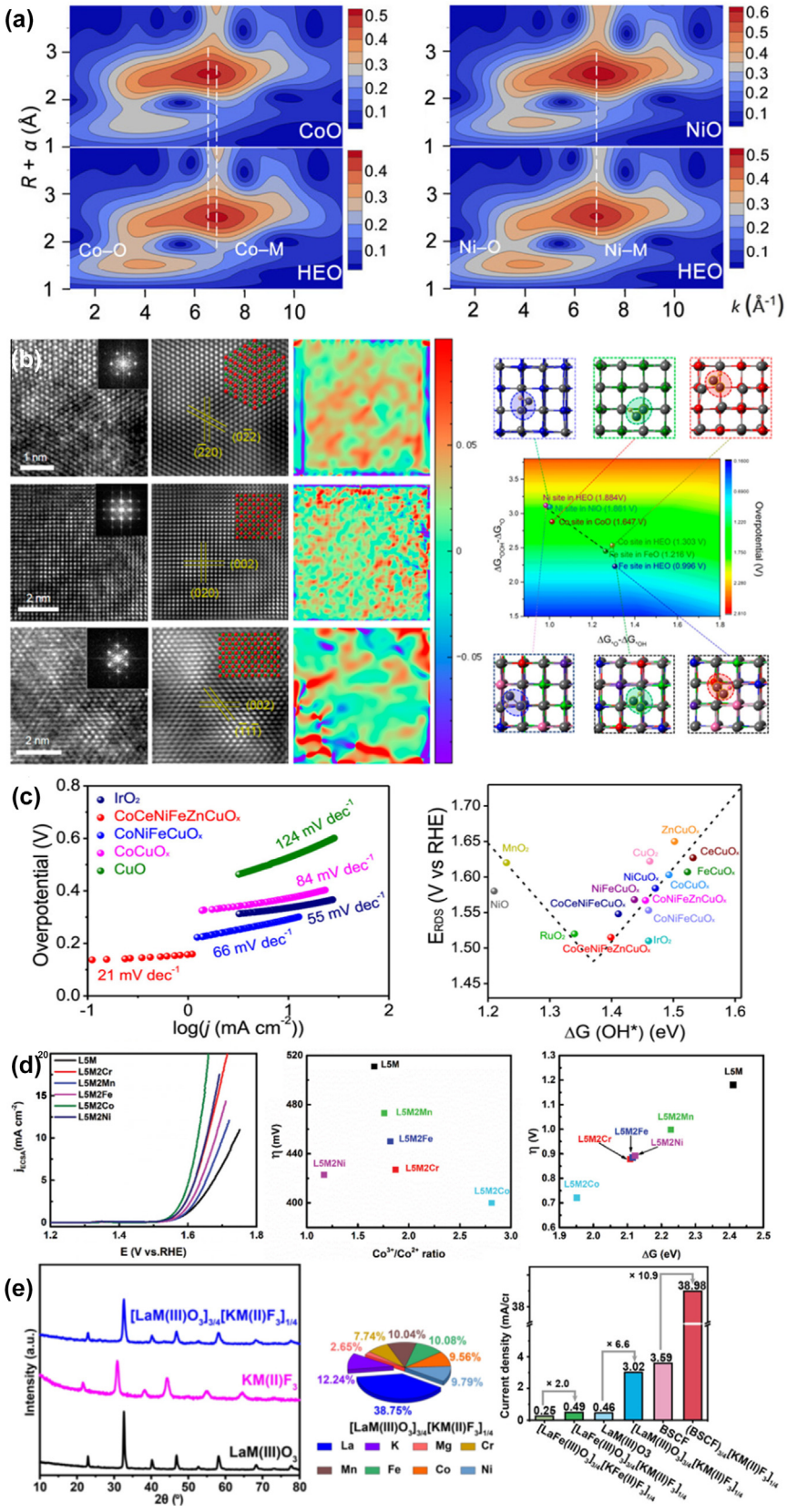

FIG. 5

a) Comparison of co/ni-o lengths in heo and corresponding oixdes. Reproduced with permission [66]. Copyright 2022, Elsevier. b) Atomic strain distribution analysis and calculated overpotentials of HEO. Reproduced with permission [76]. Copyright 2022, ACS. c) Tafel plots and volcano plot of HEOs and comparing materials. Reproduced with permission [95]. Copyright 2020, ACS. d) Property comparison in La(CrMnFeCoNi)O_3 system. Reproduced with permission [128]. Copyright 2021, Wiley-VCH. e) The XRD patterns and OER properties of high entropy oxide/fluoride and their solid solution. Reproduced with permission [130]. Copyright 2021, Wiley-VCH.

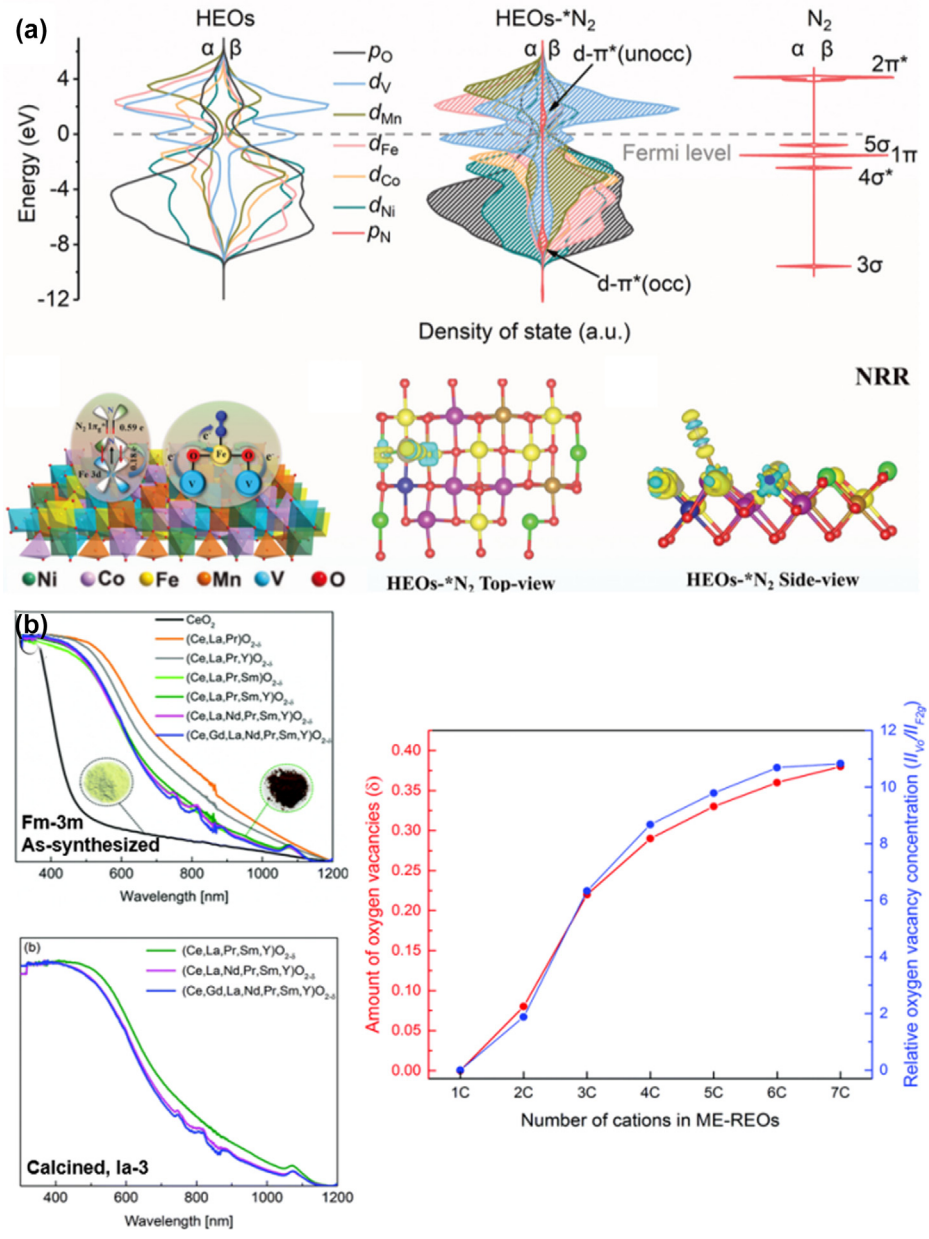

FIG. 6

a) Predicted NRR activities for sea urchin shaped HEO nanocatalyst $(Ni_{0.20}Co_{0.16}Fe_{0.24}Mn_{0.18}V_{0.22})_3O_4$. Reproduced with permission [82]. Copyright 2022, Wiley-VCH. b) UV–Vis absorption spectra and oxygen vacancy concentration of $(CeGdLaNdPrSmY)O_{2-\delta}$ system. Reproduced with permission [79]. Copyright 2017, RSC.

entropy $Pb(ZrTi)_{0.5}O_3$ performed worse in stability and selectivity of two electron ORR reaction [136]. The released lattice strain and reduced electron migration capability detected by in situ Raman could be the reason of such differences. This bifunctional catalyst also had fenton reaction activities, which degraded pollutants using the as-produced H_2O_2 in ORR.

Mascotto's team reported a $[La_{0.4}Sr_{0.6-\alpha}][Ti_{0.6}Fe_{0.35}Ni_{0.05}]O_{3\pm\delta}$ catalyst with metallic active sites formed by exsolution during catalysis [137]. The HEO support has advantages including oxygen vacancies and tunable Fe-Ni ratio by changing the Sr content, bimetallic Fe-Ni sites prefer oxidative dehydrogenation of ethane rather than ethane reforming in the present of Fe(0) sites.

Photocatalysis

Edalati and coauthors reported a mixture of monoclinic (AB_2O_7) and orthorhombic $(A_6B_2O_{17})$ type perovskites with formula of $(TiZrHfNbTa)_5O_{11}$, the HEOs had enhanced visible adsorption and bandgap as 2.9 eV, exhibited photocatalytic activity for water splitting and CO reduction [57]. Spinel HEO $(GaCrMnNiZn)_3O_4$ was synthesized by Wang's team and after calcining at different temperature, with narrow bandgap of 1.53 to 1.64 eV [138]. The catalyst with treatment at 800 °C possessed the highest activity in photocatalytic CO_2 reduction.

Sarkar and coauthors started from compound $(CePr)O_{2-\delta}$, designed a series of rare earth oxides of the $(CeGdLaNdPrSmY)O_{2-\delta}$ system by adding element one by one and tested their

potential in photocatalysis [79]. A phase transition from *Fm-3m* to *Ia-3* after calcined at 1000 °C was observed when the oxide is HEO at the condition of 5–7 elements. Since all elements other than Ce and Pr are trivalent, the δ becomes larger as the number of elements increased, consistent with the measured change in amount of oxygen vacancies, produced a lower band gap in the visible light (Fig. 6b). Wu's team reported piezo-photocatalytic properties for dye decomposition using $(Ca_xZrYCeCr)O_2$ with ferroelectricity [139].

The status quo of HEOs to catalytic applications

Despite the promising catalytic applications, should recognize that the performance of the current HEOs basically follows the "cocktail" effect, where the performance of HEOs still highly depends on the intrinsic activity with effort from synergies. Non-equimolar ratio in HEO system may still be more beneficial for catalytic applications despite of the highest configuration entropy, despite of the entropy effect. There is no coincidence that the HEO catalysts possess the same catalytic applications and similar reaction pathway as specific one or several components. The initial progress in these reactions has been facilitated by these active elements, as the mainstream research ideas reflect that creating HEO based catalyst still relies on simple strategies, such as adding elements and finding analogues based on the existed catalytic materials. Thus, the industrial potential of these applications has yet to be fully realized.

In summary, electrocatalysis studies focused on the rock salt, spinel, and perovskite type HEOs mainly composed of transition metals, some of which are inherently active in alkaline OER reactions [140]. While photocatalysis studies prefer fluorites type mainly composed of rare earth elements, especially Ce, its oxide has visible photocatalytic properties [141]. HEOs containing elements with variable valence are found to be effective in oxidation reactions, such as Ce, Cu, Co, etc., nevertheless, their oxides also exhibited CO oxidation properties as the probe reaction [142]. Monovalent Cu appears in CO environment and has good resistant to vapor, which is in consistent with prior reports [120]. And some elements seem having the higher weight in determining the properties. As motioned above, Ce and Pr are able to stabilize the fluorite structure with strongly favor of phase formation of fluorite. But the fascinated properties from unexceptional synergies were rarely discovered for HEOs.

It's still early to assert that HEOs could reduce the cost of catalysts. Active components are always expensive due to the reserves of mineral, supply and demand, and whether existing other applications. Mineral resources are not evenly distributed among countries and for example, during the COVID-19, the prices of most precious metals fluctuated greatly, due to the impact of supply, which the is limited to a few production areas and not heavily stored by the downstream industries. Comparing to the catalysts with active element as the major component, HEO could significantly lower the price of raw materials by reducing the usage of monocomponent, where some cheap elements filled in. However, HEOs with high ratio of "inactive" elements, such as Mg for battery anode or Cr and Mn for OER [129], may perform less well even than single component materials. For supported precious metal catalysts, the cost is dominated by their loading amount, rather than the substrates. Additionally, the recycling of HEOs could be challenge owing to the separation process of the multicomponents.

Discussion

Prediction new HEOs

The formation of new HEOs is full of challenges as viable combinations of elements can be scarce, despite a large number of possible combinations. Analogously, according to a search of the simulated materials database AFLOW, very few viable combinations of metals exhibited entropy stabilization from increasing the number to offset enthalpy [143]. Thus, more mechanistic investigations on both short- and long-range disorder are necessary. The assumption that cations in HEOs are completely disordered overlooks the impact of factors such as charge interactions, radii differences, and dislocation on material entropy. In designing new HEO materials and HEO supported SACs, strategies focusing building blocks can be adopted. As far as we know, the stability of HEO is highly dependent on the ionic radius. The significant differences in the ionic radii among transition metals present a challenge for discovery of new HEOs. Nevertheless, the concentrated radius resulting from lanthanide contraction in rare earth elements may provide opportunities for the discovery of previously unknown HEO materials. Considering this, Dong's team presented a material design method based on cluster model for optimizing the rutile type HEOs containing Ti, Sn, Nb, Ta and Ga/Fe/Cr (Fig. 7a) [144]. Block strategy connects small domain associating multiple atoms with long-range lattice periodicity and distribution disorder, which simplifies the amount of configurations. The results will facilitate the understanding of interatom relationships [145–148] and help in identifying more factors affecting stability from a multicomponent perspective. Novel HEO supported SACs could also be design based on the metal pairs, undercoordinated atom sites or coordination in higher shells for more accurate microenvironment regulation.

Moreover, algorithms become more important in theorical studies [149]. Computer clusters enable the parallel searching of materials and predicting of properties *via* DFT calculations. Multistep filtering strategy based on randomization and iterated local search (Fig. 7b) have been demonstrated in some researches [150]. However, current strategies may be inefficient due to limitations in computer performance (unfortunately, it is reaching the bottleneck) and material complexity. Therefore, new algorithms capable of handling larger datasets and more complex models describing the disorder condition of HEMs are highly demanded. Fortunately, machine learning-assisted design along with robotic high-throughput synthesis and screening (Fig. 7c) technique [151] holds promise in developing new HEO materials and optimizing catalysts. Velasco and coauthors adopted materials library with the aid of machine learning and robotic high throughput synthesis, more than 100 samples of $(CePrLaSmY)O_{2-\delta}$ are tested (Fig. 7d) and the phase, oxygen vacancy and the direct band gap are examined [151]. The research revealed more on inter-element interactions in multicomponent beyond focusing on single element by a traditional viewpoint based on strategy of elemental addition and deletion in synthesis.

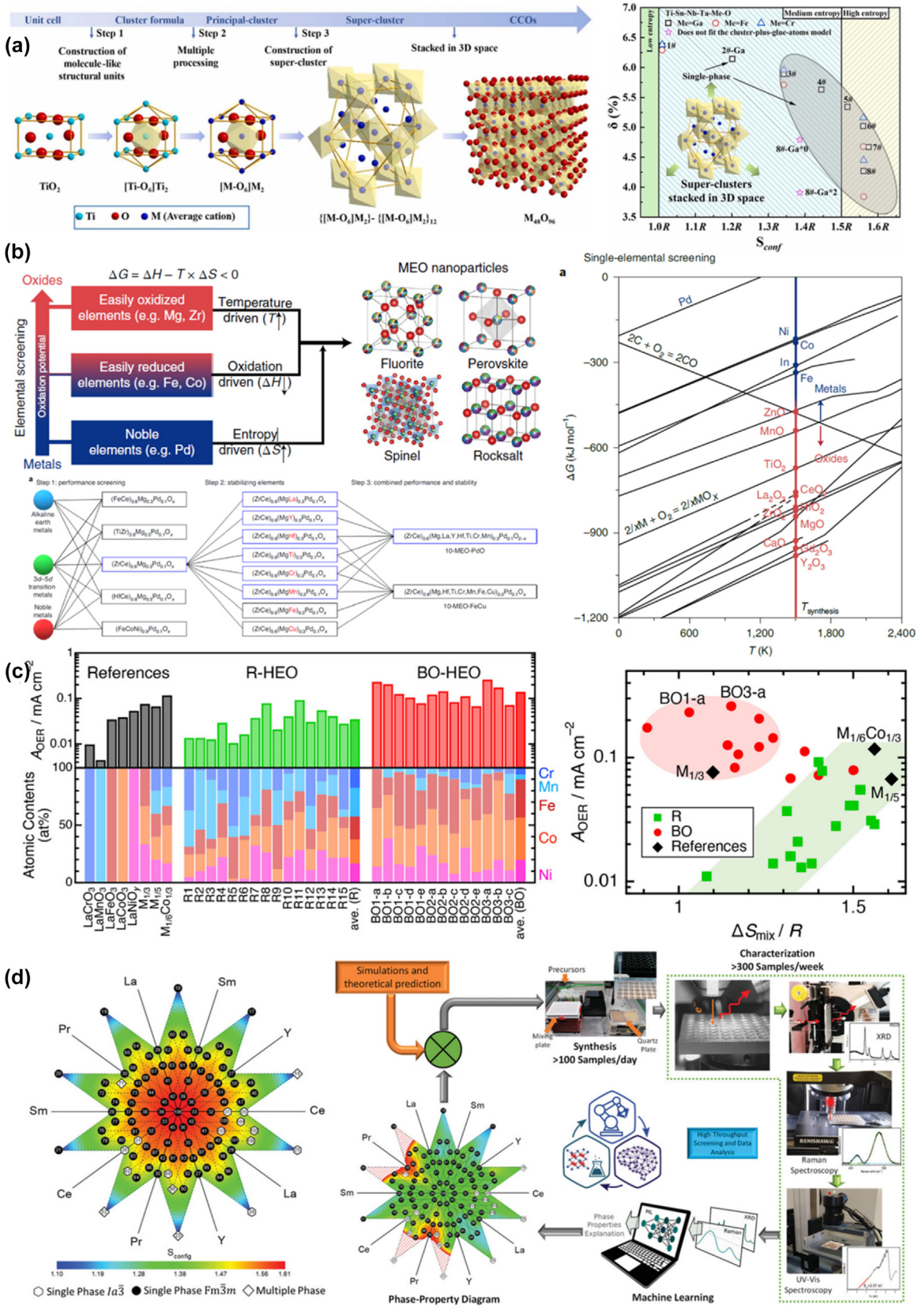

FIG. 7

Schematic illustration of HEO design strategies. a) Cluster model-based design strategy. Reproduced with permission [144]. Copyright 2022, Elsevier. b) Multistep filtering strategy. Reproduced with permission [69]. Copyright 2021, Springer Nature. c) Iterated local search strategy. Reproduced with permission [129]. Copyright 2022, ACS. d) High-throughput synthesis and screening strategy. Reproduced with permission [151]. Copyright 2021, Wiley-VCH.

Combining HEO with SAC

SACs feature maximized atom-utilization efficiency, unique selectivity and poisoning resistance, inheriting both advantages from homogeneous and heterogeneous catalysis, which innovates the catalysis field in past decade [152–154]. By adopting HEOs as supports, active materials such as precious metals could be introduced and further atomically dispersed, solving the problem of low activity that plagues current researches of HEOs [155]. SACs loaded on HEO take advantage of the enhanced effects and make most of the wide adjustability from high entropy structure, also arise the unique coordination environments and electronic structures themselves. The combination of both exhibits high industrial potential. But so far, there are still limited reports of SAC/HEO materials, probably due to the high tendency of aggregation of dispersed precious metal atoms on ordinary oxides under high temperature. Some synthetic procedures of SAC could perform at the temperature of HEO synthesis. For example, ceria showed ability trapping single atoms during calcination [156] and similar strategy may also works for other flourite type HEOs. Fortunately, a considerable number of SACs are fabricated by post-synthetic methods and avoid annealing process, which remain possibility in extending the methods to SAC/HEO hybrid material synthesis. On the other hand, HEOs have the potential instead to overcome the difficulties the traditional oxide-based SACs facing, such as poor loading capacity, low high-temperature stability and serious leaching. Their advantages of rich defects, abundant oxygen vacancies and enough stability against catalytic atmosphere not only meet the criteria for atomic stabilization but also contribute to an enhanced metal-support interaction [157,158], which even promoting better properties of SACs. The surface reconstruction ability also enables self-refreshing of active sites and redispersion of SACs owing to high-temperature favored dynamic structure of HEOs.

Perspective for HEOs in nanocatalysis

HEO has brought innovative ideas to nanocatalyst design. By just replacing the component of specific site with ≥ 5 major components, if the oxide remains a single phase, it probably gain from the multiple effects, exhibiting advantages including abundant lattice oxygen, high density of dislocation and defects, corrosion resistance properties, amorphous like properties, acceptable stability and self-regenerated properties, which are beneficial to catalysis. More importantly, HEOs provide wide adjustability and complexity in localized environments owing to the multi-component. By exploring synthetic procedures in extreme conditions and fast quenching methods to achieve valence combinations and non-trivial structure design, there is great hope to obtain novel catalyst systems, aiming to solve long-standing problems in vision of catalysis, such as selective oxidation and activation of C—H bonds [159,160]. At the same time, the mechanisms involved in current HEO systems still remain largely unstudied. Same as the ordinary oxide based catalytic materials, characteristics including specific surface area, defects, facets, etc. also influence the of activities of HEOs, demanding systematic researches. The revolution in technique may bring possibility to obtain information about electron density, valence states, lattice distortion, vacancies, etc., which enhances the understanding and answer the numerous unknowns about the formation and mechanism in HEOs.

Systematic study of these properties and find green synthesis strategies to achieve large-scale, low cost and morphology controllable production of HEOs are another challenge but more confident to achieve breakthrough in the short-term. The goal is beneficially for the improvement of existing catalytic systems and has high application prospects in oxophilnic reactions [161] especially for nanozymes [162], OER and CO_2 reduction [163]. Moreover, HEOs can serve as not only catalysts but also ideal supports for metallic active sites, opening up new avenues for research and industrial applications in thermo-, electro-, and photocatalysis.

Data availability

Data will be made available on request.

Declaration of Competing Interest

The authors declare that they have no known competing financial interests or personal relationships that could have appeared to influence the work reported in this paper.

Acknowledgements

This work was supported by the National Key R&D Program of China (2018YFA0702003), the National Natural Science Foundation of China (22102128, 22279097, 22002185) and Science and Technology Key Project of Guangdong Province of China (2020B010188002), and the China Postdoctoral Science Foundation (2021TQ0172, 2022M711793). Qishun Wang acknowledged financial support from the Shuimu Tsinghua Scholar Program.

References

[1] B. Cantor et al., Mater. Sci. Eng. A 375–377 (2004) 213–218, https://doi.org/10.1016/j.msea.2003.10.257.
[2] J.-W. Yeh et al., Adv. Eng. Mater. 6 (2004) 299–303, https://doi.org/10.1002/adem.200300567.
[3] Y. Sun et al., Matter. (2022), https://doi.org/10.1016/j.matt.2022.09.023.
[4] T.A.A. Batchelor et al., Joule. 3 (2019) 834–845, https://doi.org/10.1016/j.joule.2018.12.015.
[5] Y. Zhang, High-Entropy Materials A Brief Introduction, Springer, Singapore, 2019.
[6] W. Zhang, P.K. Liaw, Y. Zhang, Sci. China Mater. 61 (2018) 2–22, https://doi.org/10.1007/s40843-017-9195-8.
[7] B. Cantor, Prog. Mater Sci. 120 (2021), https://doi.org/10.1016/j.pmatsci.2020.100754 100754.
[8] Z. Lei et al., Scr. Mater. 165 (2019) 164–169, https://doi.org/10.1016/j.scriptamat.2019.02.015.
[9] Y. Zhou et al., Nano Res. (2023), https://doi.org/10.1007/s12274-023-5419-2.
[10] X. Li et al., Nano Res. (2022), https://doi.org/10.1007/s12274-022-5207-4.
[11] Y. Pan et al., Chem. Eng. J. 451 (2023), https://doi.org/10.1016/j.cej.2022.138659 138659.
[12] S.H. Albedwawi et al., Mater. Des. 202 (2021), https://doi.org/10.1016/j.matdes.2021.109534 109534.
[13] X. Liu et al., Nano Res. (2023), https://doi.org/10.1007/s12274-022-5259-5.
[14] Y. Lei et al., Nano Res. 15 (2022) 6054–6061, https://doi.org/10.1007/s12274-022-4304-8.
[15] J. Xing et al., Nano Res. 16 (2023) 2486–2494, https://doi.org/10.1007/s12274-022-5020-0.
[16] T.X. Nguyen et al., Adv. Sci. 8 (2021) 2002446, https://doi.org/10.1002/advs.202002446.
[17] S. Jiang et al., J. Colloid Interface Sci. 606 (2022) 635–644, https://doi.org/10.1016/j.jcis.2021.08.060.

[18] Z. Jia et al., ACS Mater. Lett. 4 (2022) 1389–1396, https://doi.org/10.1021/acsmaterialslett.2c00371.
[19] Z. Jia et al., Adv. Funct. Mater. 31 (2021) 2101586, https://doi.org/10.1002/adfm.202101586.
[20] W.-T. Koo et al., ACS Nano 14 (2020) 6407–6413, https://doi.org/10.1021/acsnano.0c03993.
[21] Q. Wang et al., Small 18 (2022) 2204135, https://doi.org/10.1002/smll.202204135.
[22] Z. Jia et al., Adv. Mater. 32 (2020) 2000385, https://doi.org/10.1002/adma.202000385.
[23] Y. Han et al., Nat. Commun. 13 (2022) 2871, https://doi.org/10.1038/s41467-022-30260-4.
[24] C.M. Rost et al., Nat. Commun. 6 (2015) 8485, https://doi.org/10.1038/ncomms9485.
[25] Y. Sun, S. Dai, Sci. Adv. 7 (2021) eabg1600, https://doi.org/10.1126/sciadv.abg1600.
[26] Y. Yao et al., Sci. Adv. 6 (2020) eaaz0510, https://doi.org/10.1126/sciadv.aaz0510.
[27] S.J. McCormack, A. Navrotsky, Acta Mater. 202 (2021) 1–21, https://doi.org/10.1016/j.actamat.2020.10.043.
[28] O.F. Dippo, K.S. Vecchio, Scr. Mater. 201 (2021), https://doi.org/10.1016/j.scriptamat.2021.113974 113974.
[29] X. Shi et al., Phys. B Condens. Matter 666 (2023), https://doi.org/10.1016/j.physb.2023.415140 415140.
[30] M. Pianassola et al., J. Adv. Ceram. 11 (2022) 1479–1490, https://doi.org/10.1007/s40145-022-0625-z.
[31] E.P. George, D. Raabe, R.O. Ritchie, Nat. Rev. Mater. 4 (2019) 515–534, https://doi.org/10.1038/s41578-019-0121-4.
[32] C. Oses, C. Toher, S. Curtarolo, Nat. Rev. Mater. 5 (2020) 295–309, https://doi.org/10.1038/s41578-019-0170-8.
[33] S. Akrami et al., Mater. Sci. Eng. R. Rep. 146 (2021), https://doi.org/10.1016/j.mser.2021.100644 100644.
[34] H. Xiang et al., J. Adv. Ceram. 10 (2021) 385–441, https://doi.org/10.1007/s40145-021-0477-y.
[35] Y. Ma et al., Energ. Environ. Sci. 14 (2021) 2883–2905, https://doi.org/10.1039/D1EE00505G.
[36] Y. Wang, Y. Wang, Nano Energy 104 (2022), https://doi.org/10.1016/j.nanoen.2022.107958 107958.
[37] J.L. Braun et al., Adv. Mater. 30 (2018) 1805004, https://doi.org/10.1002/adma.201805004.
[38] L. Sun et al., Mater. Res. Lett. 8 (2020) 424–430, https://doi.org/10.1080/21663831.2020.1783007.
[39] L. Tang et al., J. Am. Ceram. Soc. 104 (2021) 1953–1958, https://doi.org/10.1111/jace.17659.
[40] M. Fracchia et al., Scr. Mater. 188 (2020) 26–31, https://doi.org/10.1016/j.scriptamat.2020.07.002.
[41] A. Sarkar et al., J. Eur. Ceram. Soc. 38 (2018) 2318–2327, https://doi.org/10.1016/j.jeurceramsoc.2017.12.058.
[42] H. Chen et al., Chem. Commun. 56 (2020) 15056–15059, https://doi.org/10.1039/D0CC05860B.
[43] H. Chen et al., Appl. Catal. B Environ. 276 (2020), https://doi.org/10.1016/j.apcatb.2020.119155 119155.
[44] K.-P. Tseng et al., J. Am. Ceram. Soc. 103 (2020) 569–576, https://doi.org/10.1111/jace.16689.
[45] J. Sun et al., J. Eur. Ceram. Soc. 42 (2022) 5053–5064, https://doi.org/10.1016/j.jeurceramsoc.2022.05.007.
[46] B. Han et al., Angew. Chem. Int. Ed. 59 (2020) 11824–11829, https://doi.org/10.1002/anie.202003208.
[47] X. Zhou et al., Adv. Mater. 34 (2022) 2201859, https://doi.org/10.1002/adma.202201859.
[48] P. Zhu, X. Xiong, D. Wang, Nano Res. 15 (2022) 5792–5815, https://doi.org/10.1007/s12274-022-4265-y.
[49] B. Qiao et al., Nat. Chem. 3 (2011) 634–641, https://doi.org/10.1038/nchem.1095.
[50] Y. Xiong et al., Nano Res. 14 (2021) 2418–2423, https://doi.org/10.1007/s12274-020-3244-4.
[51] X. Zheng et al., Angew. Chem. Int. Ed. (2023) e202217449, https://doi.org/10.1002/anie.202217449.
[52] J. Yang et al., Angew. Chem. Int. Ed. 61 (2022) e202200366.
[53] X. Zheng et al., Nano Res. 15 (2022) 7806–7839, https://doi.org/10.1007/s12274-022-4429-9.
[54] W.-H. Li et al., Angew. Chem. Int. Ed. 61 (2022) e202209749.
[55] B. Xiao et al., Nano Energy 95 (2022), https://doi.org/10.1016/j.nanoen.2022.106962 106962.
[56] S. Nie et al., Nano Res. 15 (2022) 4867–4872, https://doi.org/10.1007/s12274-021-3803-3.
[57] P. Edalati et al., J. Mater. Chem. A 8 (2020) 3814–3821, https://doi.org/10.1039/C9TA12846H.
[58] Y. Xing et al., J. Mater. Sci. Technol. 103 (2022) 215, https://doi.org/10.1016/j.jmst.2021.06.057.
[59] K. Kusada et al., Angew. Chem. Int. Ed. 61 (2022) e202209616.
[60] H. Xu et al., Nat. Commun. 11 (2020), https://doi.org/10.1038/s41467-020-17738-9.
[61] S. Hou et al., Nat. Commun. 12 (2021) 5917, https://doi.org/10.1038/s41467-021-26160-8.
[62] K. Liu et al., Sci. Adv. 8 (2022) eabn2030, https://doi.org/10.1126/sciadv.abn2030.
[63] J. Wei et al., Nano Res. (2021), https://doi.org/10.1007/s12274-021-3860-7.
[64] D. Feng et al., Angew. Chem. Int. Ed. 59 (2020) 19503–19509, https://doi.org/10.1002/anie.202004892.
[65] S.L. Fereja et al., ACS Appl. Mater. Interfaces 14 (2022) 38727–38738, https://doi.org/10.1021/acsami.2c09161.
[66] F. Liu et al., Chin. J. Catal. 43 (2022) 122, https://doi.org/10.1016/S1872-2067(21)63794-4.
[67] A. Gautam, M.I. Ahmad, Ceram. Int. 47 (2021) 22225–22228, https://doi.org/10.1016/j.ceramint.2021.04.128.
[68] J. Dąbrowa et al., J. Eur. Ceram. Soc. 41 (2021) 3844–3849, https://doi.org/10.1016/j.jeurceramsoc.2020.12.052.
[69] T. Li et al., Nat. Catal. (2021) 1–9, https://doi.org/10.1038/s41929-020-00554-1.
[70] Y. Yao et al., Science 359 (2018) 1489–1494, https://doi.org/10.1126/science.aan5412.
[71] L. Song et al., J. Materiomics 5 (2019) 436–445, https://doi.org/10.1016/j.jmat.2019.02.003.
[72] J. Johny et al., Nano Res. 15 (2022) 4807–4819, https://doi.org/10.1007/s12274-021-3804-2.
[73] M. Biesuz et al., J. Asian Ceram. Soc. 7 (2019) 127–132, https://doi.org/10.1080/21870764.2019.1595931.
[74] X. Wang et al., Mater. Today 35 (2020) (2000) 106–114, https://doi.org/10.1016/j.mattod.2019.11.004.
[75] Y. Yu et al., J. Mater. Chem. A 10 (2022) 21260–21265, https://doi.org/10.1039/D2TA06128G.
[76] H. Wu et al., Nano Lett. 22 (2022) 6492–6500, https://doi.org/10.1021/acs.nanolett.2c01147.
[77] Z. Zhang et al., Chem. Mater. 31 (2019) 5529–5536, https://doi.org/10.1021/acs.chemmater.9b01244.
[78] X. Wang et al., Adv. Mater. 32 (2020) 2002853, https://doi.org/10.1002/adma.202002853.
[79] A. Sarkar et al., Dalton Trans. 46 (2017) 12167–12176, https://doi.org/10.1039/C7DT02077E.
[80] J. Li et al., Appl. Catal. B Environ. 249 (2019) 63–71, https://doi.org/10.1016/j.apcatb.2019.02.060.
[81] Q. Wang et al., Nano Res. 15 (2022) 8751–8759, https://doi.org/10.1007/s12274-022-4179-8.
[82] Y. Sun et al., Small 18 (2022) 2106358, https://doi.org/10.1002/smll.202106358.
[83] G. Wang et al., ACS Appl. Mater. Interfaces 12 (2020) 45155–45164, https://doi.org/10.1021/acsami.0c11899.
[84] D. Wang et al., J. Mater. Chem. A 7 (2019) 24211–24216, https://doi.org/10.1039/C9TA08740K.
[85] H. Yu et al., Sci. Adv. 8 (2022) eabq2356, https://doi.org/10.1126/sciadv.abq2356.
[86] Y. Shi et al., Nanoscale 14 (2022) 7817–7827, https://doi.org/10.1039/D1NR08316C.
[87] K. Iwase, I. Honma, ACS Appl. Energy Mater. 5 (2022) 9292–9296, https://doi.org/10.1021/acsaem.2c01751.
[88] X. He et al., Cell Rep. Phys. Sci. (2019), https://doi.org/10.1016/j.xcrp.2019.100004 100004.
[89] H. Chen et al., ACS Mater. Lett. 1 (2019) 83–88, https://doi.org/10.1021/acsmaterialslett.9b00064.
[90] J. Zhao et al., ACS Catal. 11 (2021) 12247–12257, https://doi.org/10.1021/acscatal.1c03228.
[91] F. Okejiri et al., ChemSusChem 13 (2020) 111–115, https://doi.org/10.1002/cssc.201902705.

[92] Z. Jin et al., Small 18 (2022) 2107207, https://doi.org/10.1002/smll.202107207.
[93] Y. Zhang et al., Nanoscale 13 (2021) 16164–16171, https://doi.org/10.1039/D1NR03539H.
[94] Z. Jin et al., Chem. Mater. 33 (2021) 1771–1780, https://doi.org/10.1021/acs.chemmater.0c04695.
[95] W. Huang et al., ACS Nano 14 (2020) 17640–17651, https://doi.org/10.1021/acsnano.0c08571.
[96] P. Ghigna et al., ACS Appl. Mater. Interf. 12 (2020) 50344–50354, https://doi.org/10.1021/acsami.0c13161.
[97] M.R. Chellali et al., Scr. Mater. 166 (2019) 58–63, https://doi.org/10.1016/j.scriptamat.2019.02.039.
[98] R. Hu, S. Jin, G. Sha, Prog. Mater Sci. 123 (2022), https://doi.org/10.1016/j.pmatsci.2021.100854 100854.
[99] A. Farhan et al., Phys. Rev. B 106 (2022) L060404, https://doi.org/10.1103/PhysRevB.106.L060404.
[100] J. Zhang et al., Chem. Mater. 31 (2019) 3705–3711, https://doi.org/10.1021/acs.chemmater.9b00624.
[101] L. Su et al., Nat. Commun. 13 (2022) 2358, https://doi.org/10.1038/s41467-022-30018-y.
[102] L. Su et al., ACS Nano 16 (2022) 21397–21406, https://doi.org/10.1021/acsnano.2c09760.
[103] G. Anand et al., Acta Mater. 146 (2018) 119–125, https://doi.org/10.1016/j.actamat.2017.12.037.
[104] Z. Lun et al., Nat. Mater. 20 (2021) 214–221, https://doi.org/10.1038/s41563-020-00816-0.
[105] F. Ding et al., JACS 144 (2022) 8286–8295, https://doi.org/10.1021/jacs.2c02353.
[106] J. Dąbrowa et al., Mater. Lett. 216 (2018) 32–36, https://doi.org/10.1016/j.matlet.2017.12.148.
[107] A. Sarkar et al., Acta Mater. 226 (2022) 117581, https://doi.org/10.1016/j.actamat.2021.117581.
[108] G. Dai et al., J. Mater. Sci. Technol. 116 (2022) 11, https://doi.org/10.1016/j.jmst.2021.11.032.
[109] K. Chen et al., Ceram. Int. 47 (2021) 21207–21211, https://doi.org/10.1016/j.ceramint.2021.04.123.
[110] M. Pianassola et al., J. Am. Ceram. Soc. 103 (2020) 2908–2918, https://doi.org/10.1111/jace.16971.
[111] L. Spiridigliozzi et al., Acta Mater. 202 (2021) 181–189, https://doi.org/10.1016/j.actamat.2020.10.061.
[112] A.J. Wright et al., Acta Mater. 211 (2021), https://doi.org/10.1016/j.actamat.2021.116858 116858.
[113] C. Riley et al., ACS Appl. Mater. Interfaces 13 (2021) 8120–8128, https://doi.org/10.1021/acsami.0c17446.
[114] M. Fracchia et al., J. Phys. Chem. Lett. 11 (2020) 3589–3593, https://doi.org/10.1021/acs.jpclett.0c00602.
[115] Y. Sun et al., ACS Cent. Sci. 8 (2022) 1081–1090, https://doi.org/10.1021/acscentsci.2c00340.
[116] S. Zhao et al., ACS Appl. Mater. Interfaces 13 (2021) 48764–48773, https://doi.org/10.1021/acsami.1c14456.
[117] H. Chen et al., J. Mater. Chem. A 6 (2018) 11129–11133, https://doi.org/10.1039/C8TA01772G.
[118] B. Hu et al., Adv. Mater. 34 (2022) 2107721, https://doi.org/10.1002/adma.202107721.
[119] B. Song et al., Nano Res. 15 (2022) 5922–5932, https://doi.org/10.1007/s12274-022-4251-4.
[120] Y. Shu et al., AIChE J 67 (2021) e17046.
[121] D. Zhou et al., Nano Res. 15 (2022) 3575–3586, https://doi.org/10.1007/s12274-021-3901-2.
[122] Q. Wang et al., Small Struct. 3 (2022) 2200059, https://doi.org/10.1002/sstr.202200059.
[123] C. Wang et al., Nanoscale 15 (2023) 8619–8632, https://doi.org/10.1039/D2NR07195A.
[124] X. Zheng et al., Angew. Chem. Int. Ed. 61 (2022) e202205946.
[125] Y. Gao, B. Liu, D. Wang, Adv. Mater. (2023) 2209654, https://doi.org/10.1002/adma.202209654.
[126] J. Xia et al., Mater. Today 53 (2022) 217–237, https://doi.org/10.1016/j.mattod.2021.11.022.
[127] Z. Zeng et al., Chem. Soc. Rev. 49 (2020) 1109–1143, https://doi.org/10.1039/C9CS00330D.
[128] T.X. Nguyen et al., Adv. Funct. Mater. 31 (2021) 2101632, https://doi.org/10.1002/adfm.202101632.
[129] Y. Okazaki et al., Chem. Mater. 34 (2022) 10973–10981, https://doi.org/10.1021/acs.chemmater.2c02986.
[130] T. Wang et al., Angew. Chem. Int. Ed. 60 (2021) 9953–9958, https://doi.org/10.1002/anie.202101120.
[131] L. Tang et al., Chem. Eng. J. 417 (2021), https://doi.org/10.1016/j.cej.2021.129324 129324.
[132] L. Tang et al., Adv. Funct. Mater. 32 (2022) 2112157, https://doi.org/10.1002/adfm.202112157.
[133] K.L. Svane, J. Rossmeisl, Angew. Chem. Int. Ed. 61 (2022) e202201146.
[134] S. He et al., Nano Res. 15 (2022) 4785–4791, https://doi.org/10.1007/s12274-021-3665-8.
[135] H. Nan et al., Chem. Eng. J. 452 (2023), https://doi.org/10.1016/j.cej.2022.139501 139501.
[136] Z. Chen et al., Angew. Chem. Int. Ed. 61 (2022) e202200086.
[137] A.I. Tsiotsias et al., ACS Nano 16 (2022) 8904–8916, https://doi.org/10.1021/acsnano.1c11111.
[138] Z. Jiang et al., Appl. Surf. Sci. 612 (2023), https://doi.org/10.1016/j.apsusc.2022.155809 155809.
[139] S.C. Chang et al., Appl. Catal. B Environ. 324 (2023), https://doi.org/10.1016/j.apcatb.2022.122204 122204.
[140] T. Wu et al., Nat. Commun. 12 (2021) 3634, https://doi.org/10.1038/s41467-021-23896-1.
[141] Q. Wang, Z. Pan, Nano Res. 15 (2022) 10090–10109, https://doi.org/10.1007/s12274-022-4705-8.
[142] L. Kang et al., Angew. Chem. Int. Ed. 60 (2021) 14420–14428, https://doi.org/10.1002/anie.202102570.
[143] C. Toher et al., npj Comput. Mater. 5 (2019) 1–3, https://doi.org/10.1038/s41524-019-0206-z.
[144] Y. Yu et al., J. Alloy. Compd. 926 (2022), https://doi.org/10.1016/j.jallcom.2022.166771 166771.
[145] W.-H. Li, J. Yang, D. Wang, Angew. Chem. Int. Ed. 61 (2022) e202213318.
[146] Y. Wang et al., Angew. Chem. Int. Ed. 62 (2023) e202219191.
[147] H. Jing et al., Adv. Powder Mater. (2021), https://doi.org/10.1016/j.apmate.2021.10.004 100013.
[148] Y. Wang et al., Angew. Chem. Int. Ed. 61 (2022) e202115735.
[149] Z. Lu, Z.W. Chen, C.V. Singh, Matter. 3 (2020) 1318–1333, https://doi.org/10.1016/j.matt.2020.07.029.
[150] O.A. Krysiak et al., Nano Res. 15 (2022) 4780–4784, https://doi.org/10.1007/s12274-021-3637-z.
[151] L. Velasco et al., Adv. Mater. 33 (2021) 2102301, https://doi.org/10.1002/adma.202102301.
[152] H. Jia et al., Small 18 (2022) 2200036, https://doi.org/10.1002/smll.202200036.
[153] Z. Zhang et al., Angew. Chem. Int. Ed. 62 (2023) e202215136.
[154] T. Cui et al., Angew. Chem. Int. Ed. 61 (2022) e202115219.
[155] Y. Wang, X. Zheng, D. Wang, Nano Res. 15 (2022) 1730–1752, https://doi.org/10.1007/s12274-021-3794-0.
[156] H. John Jones et al., Science 353 (2016) 150–154, https://doi.org/10.1126/science.aaf8800.
[157] K. Qi, M. Chhowalla, D. Voiry, Mater. Today 40 (2020) 173–192, https://doi.org/10.1016/j.mattod.2020.07.002.
[158] R. Li, D. Wang, Nano Res. 15 (2022) 6888–6923, https://doi.org/10.1007/s12274-022-4371-x.
[159] I.A. Samek et al., J. Catal. 384 (2020) 147–158, https://doi.org/10.1016/j.jcat.2020.02.017.
[160] G.-Q. Yang et al., Nano Res. (2023), https://doi.org/10.1007/s12274-022-5316-0.
[161] F. Wu et al., Nano Today 29 (2019), https://doi.org/10.1016/j.nantod.2019.100802 100802.
[162] Y. Wu et al., Mater. Today 52 (2022) 327–347, https://doi.org/10.1016/j.mattod.2021.10.032.
[163] J. Liu et al., Mater. Today 48 (2021) 95–114, https://doi.org/10.1016/j.mattod.2021.02.005.